

Micro-supervised Disturbance Learning: A Perspective of Representation Probability Distribution

Jielei Chu, *member, IEEE*, Jing Liu, Hongjun Wang, Hua Meng, Zhiguo Gong, *Senior member, IEEE*, Tianrui Li, *Senior member, IEEE*

arXiv:2003.06321v2 [cs.LG] 6 Oct 2021

Abstract—The instability is shown in the existing methods of representation learning based on Euclidean distance under a broad set of conditions. Furthermore, the scarcity and high cost of labels prompt us to explore more expressive representation learning methods which depends on the labels as few as possible. To address these issues, the small-perturbation ideology is firstly introduced on the representation learning model based on the representation probability distribution. The positive small-perturbation information (SPI) which only depend on two labels of each cluster is used to stimulate the representation probability distribution and then two variant models are proposed to fine-tune the expected representation distribution of RBM, namely, Micro-supervised Disturbance GRBM (Micro-DGRBM) and Micro-supervised Disturbance RBM (Micro-DRBM) models. The Kullback-Leibler (KL) divergence of SPI is minimized in the same cluster to promote the representation probability distributions to become more similar in Contrastive Divergence (CD) learning. In contrast, the KL divergence of SPI is maximized in the different clusters to enforce the representation probability distributions to become more dissimilar in CD learning. To explore the representation learning capability under the continuous stimulation of the SPI, we present a deep Micro-supervised Disturbance Learning (Micro-DL) framework based on the Micro-DGRBM and Micro-DRBM models and compare it with a similar deep structure which has not any external stimulation. Experimental results demonstrate that the proposed deep Micro-DL architecture shows better performance in comparison to the baseline method, the most related shallow models and deep frameworks for clustering.

Index Terms—Micro-supervised Disturbance Learning; representation probability distribution; small-perturbation; clustering.

1 INTRODUCTION

Learning expressive representations is a fundamental and challenging problem in machine learning area [1]. The success of

Jielei Chu, Hongjun Wang, Hua Meng, Tianrui Li (the corresponding author) are with the School of Computing and Artificial Intelligence, Southwest Jiaotong University, Chengdu 611756, China. Tianrui Li is also with National Engineering Laboratory of Integrated Transportation Big Data Application Technology, Southwest Jiaotong University, Chengdu 611756, China. e-mails: {jieleichu, huameng, wanghongjun, trli}@swjtu.edu.cn.

Jing Liu is with the School of Business, Sichuan University, Sichuan, 610065, Chengdu, China. e-mail: liujing@scu.edu.cn

Zhiguo Gong is with the State Key Laboratory of Internet of Things for Smart City, Department of Computer and Information Science, University of Macau, Macau, China. Email: fstzgg@um.edu.mo

many tasks such as person re-identification [2], zero-shot deep domain adaptation [3], visual recognition [4], fingerprint matching [5], and many others lie on deep representations of data. To this day, how to capture meaningful representation information from various data has always been the unremitting goal of machine learning. In recent years, much of the effort in researching representation learning methods goes into many new perspectives. To compare with high-dimensional representations of real-valued, compact representations aims to extract a discriminative and compressive feature. A compact representations learning (CRL) sub-network [6] based on a Faster R-CNN [7] has been successfully applied to tattoo examination. Since data usually contains complementary information from different views, multi-view representation learning is used to learn comprehensive representations [8]. For sharing representations among the data views, a shared multi-view data representation learning (SMDR) [9] model is devised for dealing with cross-modality and cross-domain event detection. Sun et al. [10] proposed a multi-view representation learning algorithm with deep Gaussian processes (MvDGPs), which integrates the advantages of multi-view representation learning and deep learning.

From the perspective of transferable representation and graph structure representation, many methods have also emerged for representational learning. To match different domain distributions and reproduce kernel Hilbert space, Long et al. [11] developed a deep adaptation networks (DAN) for domain adaptation. This transferable representation learning method enhances significantly feature transferability. Different distributions are exhibited between source domains and target in domain adaptation learning. To improve the universality of data representations, Tamaazousti et al. [12] proposed an MuLDiPNet which has capability to automatically change an initial source problem and extract new features. Graph data representation and learning has been studied recently [13]–[16]. To address the effect of some graph structure noises, Jiang et al. presented a Graph elastic Convolution Network (GeCN) [16] based on GCN [13] for semi-supervised classification (10% ~ 30% label rate).

To reduce the reliance on the labels, there are various semi-supervised learning methods in the research field of weakly supervised learning which are widely used in classification [17], [18], clustering [19], [20], discrete choice models [21], sentiment analysis [22], and so on. In these applications, semi-supervised

feature learning [23] is a critical phase to enhance the efficiencies and performances of the following learning tasks. Existing shallow semi-supervised feature learning methods [24], [25] exploit various semi-supervised strategies to improve learning efficiency and performance while minimize the use of labels. Chen et al. [25] presented a Sparse Rescaled Linear Square Regression (SRLSR) method which has capability to obtain more sparse regression coefficients for semi-supervised feature learning. Recently, there are some works which explore deep semi-supervised learning method [26], [27] to promote the capabilities of deep feature learning. In general, the conventional semi-supervised learning methods perform within a fixed feature space. The DCS [28] is an incremental deep semi-supervised learning method, which propagates information from labeled to unlabeled samples in the procedure of deep feature learning. In the DCS framework, the Co-Space stems from two CNN models by extracting features for all unlabeled and labeled samples. Sellami et al. [29] constructed a semi-supervised 3-D Convolutional Neural Network (3-D CNN) for the spectro-spatial classification. The approach not only preserves the information of the relevant spectro-spatial but also enhances the classification using few labeled samples. Xue et al. [30] proposed an efficient and fast semi-supervised DIOD method based on weakly deep semi-supervised joint sparse learning and Advanced Region Proposal Networks (ARPNs). Meng et al. [31] presented a Semi-supervised Graph Regularized Deep NMF (SGDNMF) with bi-orthogonal constraints for data representation. The bi-orthogonal constraints are introduced into the SGDNMF model on two factor matrices for improving the representation performance with a small fraction of labels. The deep semi-supervised learning procedure is used in the decision making module to maximize the diagnostic efficiency and simultaneously minimize the human interaction. Mercado et al. [32] proposed a semi-supervised learning method on Multilayer Graphs (semi-MG) using a regularizer of the generalized matrix mean. In each individual graph layer, the labeled and unlabeled samples are fused together with the encoding information. Recently, an unsupervised feature learning method [33] was developed based on ensemble learning and a shallow semi-supervised feature learning model, pcGRBM [34], was proposed. However, these model based on European distance shows somewhat instabilities. Besides instability, the semi-supervised feature learning model pcGRBM [34] still depends on a certain quantity of labels to obtain higher performance.

The motivation of this paper derives from the small-perturbation ideology of physical systems [35]. In simple terms, the original state of the physical system changes slightly under the stimulation of small disturbance. So, there are two interesting problems: 1) Whether the small disturbance can be used to stimulate the representation learning model to fine-tune the expected representation probability distribution? 2) Whether the representation learning capability can significantly improve under the continuous stimulation of small disturbance? To achieve these goals, the positive small-perturbation information (SPI) is used to stimulate the representation learning process from the perspective of representation probability distribution and two variant models are proposed to fine-tune the expected representation distribution of RBM [36], namely, Micro-supervised Disturbance GRBM (Micro-DGRBM) and Micro-supervised Disturbance RBM (Micro-DRBM) models. The SPI only depends on two labels of each cluster. Hence, we term this learning pattern as Micro-supervised Disturbance Learning (Micro-DL).

The Kullback-Leibler (KL) divergence [37] of SPI is minimized in the same cluster to promote the representation probability distributions become more similar in Contrastive Divergence (CD) learning [38]. In contrast, the KL divergence of SPI is maximized in the different clusters to enforce the representation probability distributions become more dissimilar in CD learning. Then we present a deep Micro-DL framework (see Fig. 1) to explore the effect of continuous stimulation of positive SPI based on Micro-DGRBM and Micro-DRBM models. Finally, we design the similar deep structure without the stimulation of positive SPI to compare the capability of representation learning with Micro-DL framework. Our Micro-DL method improves the stability [39] of representation learning from the perspective of representation probability distribution and significantly reduces the reliance on the labels. The contributions are as follows:

- The small-perturbation ideology is firstly introduced on the representation learning model which based on the representation probability distribution. Then the positive small-perturbation information (SPI) is used to stimulate the representation learning process from the perspective of representation probability distribution and two variant models are proposed to fine-tune the expected representation distribution of RBM. They are Micro-supervised Disturbance GRBM (Micro-DGRBM) for modeling real-valued data and Micro-supervised Disturbance RBM (Micro-DRBM) for modeling binary data, respectively.
- To explore the representation learning capability under the continuous stimulation of small disturbance, we present a deep Micro-supervised Disturbance Learning (Micro-DL) framework based on the Micro-DGRBM and Micro-DRBM models and compare it with a similar deep structure which has not any stimulation of positive SPI.
- Experimental results demonstrate that the proposed deep Micro-DL architecture shows better performance in comparison to the baseline method, the most related shallow models and deep frameworks for clustering. Furthermore, our Micro-DL method improves the stability of representation learning from the perspective of representation probability distribution and significantly reduces the reliance on the labels.

The rest of the paper is organized as follows. Section 2 introduces the theoretical background. Section 3 presents Micro-DL method, include two novel shallow micro-supervised disturbance representation learning models, learning algorithms and a novel deep Micro-DL architecture. Section 4 shows all experimental results. Finally, Section 5 summarizes our contributions.

2 BACKGROUND

2.1 Kullback-Leibler Divergence

The KL divergence [37], [40], [41] has been popularly used to measure the difference between two probability distributions. Let $P(x)$ and $Q(x)$ be two probability distributions of a discrete random variable x . The KL divergence is given by

$$\mathbf{KL}(P(x) \parallel Q(x)) = \sum_x P(x) \log \frac{P(x)}{Q(x)} \quad (1)$$

where KL divergence is always non-negative ($\mathbf{KL}(P \parallel Q) \geq 0$) and $\mathbf{KL}(P \parallel Q) = 0$ if and only if $P = Q$. In other words, KL divergence is the expectation of the logarithmic difference between

P and Q . To obtain a distribution P which is the closest to Q , we can minimize KL divergence of them.

In neural networks, the method of updating parameters often directs towards minimizing the KL divergence [42]. KL divergence is used to measure the similarity between uncertain objects, then it can be merged with learning algorithms to improve the performance [43]. In computer vision, the KL divergence is used in training rotation-invariant RBM [44] which can offer stability and consistency of representation. In variational Bayes Recurrent Neural Networks (BRNNs) [45], the KL divergence between the approximate posterior and the prior distributions is a vital component of the models.

2.2 Contrastive Divergence Learning

CD learning [38], [46] as a fast learning method has been successfully applied to train RBMs. It proximately follows the gradient of two KL divergences and is defined as

$$\mathbf{CD}_n = \mathbf{KL}(p_0||p_\infty) - \mathbf{KL}(p_n||p_\infty), \quad (2)$$

where p_0 is the data distribution, p_∞ is model distribution and p_n is the distribution of the data after running the Markov chain for n step.

In the encoding process of RBMs model, the conditional probability $p(h_j = 1|\mathbf{v})$ is given by:

$$p(h_j = 1|\mathbf{v}) = \sigma(b_j + \sum_i v_i w_{ij}), \quad (3)$$

where $\mathbf{v} = (v_1, v_2, \dots, v_i, \dots, v_n)$ is a vector of visible layer, σ is the sigmoid function, w_{ij} is the connection parameter between the hidden and visible layers, $\mathbf{b} = (b_1, b_2, \dots, b_j, \dots, b_m)$ is the bias parameter of hidden layers. In the reconstructed process of RBMs, the conditional probability $p(v_i = 1|\mathbf{h})$ is given by:

$$p(v_i = 1|\mathbf{h}) = \sigma(c_i + \sum_j h_j w_{ij}), \quad (4)$$

where $\mathbf{h} = (h_1, h_2, \dots, h_j, \dots, h_m)$ is a vector of hidden layer, $\mathbf{c} = (c_1, c_2, \dots, c_i, \dots, c_n)$, $\mathbf{W}_{n \times m}$ is the bias parameter of visible layer.

In the GRBM and its variants [34], [47], [48], the hidden layers remain unchanged binary units, but visible layer units are replaced by Gaussian linear units. The conditional probability of reconstructed process takes the form

$$p(\mathbf{v}|\mathbf{h}) = \mathcal{N}(\sum \mathbf{h}\mathbf{W}^T + \mathbf{c}, \sigma^2), \quad (5)$$

where \mathbf{c} is a connection matrix, $\mathcal{N}(\cdot)$ is a gaussian density.

For fast training RBMs, CD learning with one step Gibbs sampling (CD-1 learning) [46] is defined by:

$$\mathbf{CD}_1 = \mathbf{KL}(p_0||p_\infty) - \mathbf{KL}(p_1||p_\infty), \quad (6)$$

where p_1 is the distribution of the reconstructed data. Then the update rules of model parameters of RBMs are given by

$$w_{ij}^{(\tau+1)} = w_{ij}^{(\tau)} + \varepsilon(\langle v_i h_j \rangle_0 - \langle v_i h_j \rangle_1), \quad (7)$$

$$b_j^{(\tau+1)} = b_j^{(\tau)} + \varepsilon(\langle h_j \rangle_0 - \langle h_j \rangle_1) \quad (8)$$

and

$$c_i^{(\tau+1)} = c_i^{(\tau)} + \varepsilon(\langle v_i \rangle_0 - \langle v_i \rangle_1), \quad (9)$$

where $\langle \cdot \rangle_0$ denotes an average concerning the data distribution, $\langle \cdot \rangle_1$ denotes an average concerning the reconstructed data distribution and ε is learning rate.

3 MICRO-SUPERVISED DISTURBANCE LEARNING

In this section, we first present two novel shallow Micro-DGRBM and Micro-DRBM models, in which the positive SPI is used to stimulate the representation learning process from the perspective of representation probability distribution. To explore the representation learning capability under the continuous stimulation of SPI, we present a deep Micro-DL framework based on the Micro-DGRBM and Micro-DRBM models.

3.1 The Micro-DGRBM and Micro-DRBM Models

Let $\mathcal{V} = \{\mathbf{v}_1, \mathbf{v}_2, \dots, \mathbf{v}_i, \dots, \mathbf{v}_M\}$ be a visible layer data set of the Micro-DRBM model, where \mathbf{v}_i is the i th row vector of \mathcal{V} which represents the i th instance with n features ($\mathbf{v}_i = (v_{i1}, v_{i2}, \dots, v_{ij}, \dots, v_{in})$) and M is the number of instance vector. Each visible layer instance corresponds to a feature vector in the hidden layer. The hidden feature vector set of the Micro-DRBM model is denoted as $\mathcal{H} = \{\mathbf{h}_1, \mathbf{h}_2, \dots, \mathbf{h}_i, \dots, \mathbf{h}_M\}$, where m is the dimensionality of hidden layer and \mathbf{h}_i is the hidden feature of \mathbf{v}_i . Similarly, the visible layer data of the Micro-DGRBM model and its corresponding hidden feature sets are denoted as $\tilde{\mathcal{V}} = \{\tilde{\mathbf{v}}_1, \tilde{\mathbf{v}}_2, \dots, \tilde{\mathbf{v}}_i, \dots, \tilde{\mathbf{v}}_M\}$ and $\tilde{\mathcal{H}} = \{\tilde{\mathbf{h}}_1, \tilde{\mathbf{h}}_2, \dots, \tilde{\mathbf{h}}_i, \dots, \tilde{\mathbf{h}}_M\}$, respectively.

We randomly select only two visible layer vectors \mathbf{v}_f and \mathbf{v}_g from the visible layer data set of Micro-DRBM in each class. It is desirable that the probability distributions of hidden layer features \mathbf{h}_f and \mathbf{h}_g are similar. Thus, a similar feature distribution (SFD) set is defined as $\mathcal{SFD} = \{(\mathbf{h}_f, \mathbf{h}_g)|P(\mathbf{h}_f|\mathbf{v}_f) \text{ and } P(\mathbf{h}_g|\mathbf{v}_g) \text{ are similar}\}$ for modeling Micro-DRBM. Supposing the visible layer data set \mathcal{V} consists of K clusters, then the \mathcal{SFD} is a small set with K two-tuples. Similarly, we randomly select only two visible layer vectors $\tilde{\mathbf{v}}_f$ and $\tilde{\mathbf{v}}_g$ from the visible layer data set of Micro-DGRBM in each class. It is desirable that the probability distributions of hidden layer features $\tilde{\mathbf{h}}_f$ and $\tilde{\mathbf{h}}_g$ are also similar. Thus, another SFD set is defined as $\tilde{\mathcal{SFD}} = \{(\tilde{\mathbf{h}}_f, \tilde{\mathbf{h}}_g)|P(\tilde{\mathbf{h}}_f|\tilde{\mathbf{v}}_f) \text{ and } P(\tilde{\mathbf{h}}_g|\tilde{\mathbf{v}}_g) \text{ are similar}\}$ for modeling Micro-DGRBM. Supposing the visible layer data set $\tilde{\mathcal{V}}$ consists of \tilde{K} clusters, then the $\tilde{\mathcal{SFD}}$ is a small set with \tilde{K} two-tuples.

In consideration of the differences of feature distributions in hidden layer between two classes, a dissimilar feature distributions (DFD) set can be defined as $\mathcal{DFD} = \{(\mathbf{h}_r, \mathbf{h}_s)|P(\mathbf{h}_r|\mathbf{v}_r) \text{ and } P(\mathbf{h}_s|\mathbf{v}_s) \text{ are dissimilar}\}$ for modeling Micro-DRBM. Similarly, another DFD set can be defined as $\tilde{\mathcal{DFD}} = \{(\tilde{\mathbf{h}}_r, \tilde{\mathbf{h}}_s)|P(\tilde{\mathbf{h}}_r|\tilde{\mathbf{v}}_r) \text{ and } P(\tilde{\mathbf{h}}_s|\tilde{\mathbf{v}}_s) \text{ are dissimilar}\}$ for modeling Micro-DGRBM.

In the process of representation learning of the Micro-DRBM model, we expect the probability distribution between the elements of two-tuples in \mathcal{SFD} subset to be as similar as possible. Moreover, we also expect the probability distribution between the elements of two-tuples in \mathcal{DFD} subset to be as dissimilar as possible. To achieve these targets, the KL divergences between the elements of two-tuples in \mathcal{SFD} and \mathcal{DFD} sets are integrated into CD learning in the process of representation learning of the Micro-DRBM model. Similarly, the KL divergences between the elements of two-tuples in $\tilde{\mathcal{SFD}}$ and $\tilde{\mathcal{DFD}}$ sets can be fused into CD learning of Micro-DGRBM model.

Clearly, the above \mathcal{SFD} , $\tilde{\mathcal{SFD}}$, \mathcal{DFD} and $\tilde{\mathcal{DFD}}$ are used as SPI to stimulate the representation learning process from the perspective of representation probability distribution and then

to fine-tune the expected representation distribution. The Micro-supervised disturbance method is defined as follows:

$$\min_{\theta} \frac{1}{K_S} \sum_{\mathcal{SFD}} \mathbf{KL}(P(\mathbf{h}_f|\mathbf{v}_f) \| P(\mathbf{h}_g|\mathbf{v}_g)) - \frac{1}{K_D} \sum_{\mathcal{DFD}} \mathbf{KL}(P(\mathbf{h}_r|\mathbf{v}_r) \| P(\mathbf{h}_s|\mathbf{v}_s)), \quad (10)$$

where $(\mathbf{v}_f, \mathbf{v}_g) \in \mathcal{SFD}$ and $(\mathbf{v}_r, \mathbf{v}_s) \in \mathcal{DFD}$, $\theta = \{\mathbf{W}, \mathbf{b}, \mathbf{c}\}$ is the parameter of Micro-DRBM, K_S and K_D are the numbers of two-tuples in \mathcal{SFD} and \mathcal{DFD} sets, respectively. Under the stimulation of these Micro-supervised disturbance, we expect that the representation probability distributions become more similar and dissimilar in the same and different clusters, respectively. Similarly, the Micro-supervised disturbance method for Micro-DGRBM model is given by:

$$\min_{\tilde{\theta}} \frac{1}{K_S} \sum_{\widetilde{\mathcal{SFD}}} \mathbf{KL}(P(\widetilde{\mathbf{h}}_f|\widetilde{\mathbf{v}}_f) \| P(\widetilde{\mathbf{h}}_g|\widetilde{\mathbf{v}}_g)) - \frac{1}{K_D} \sum_{\widetilde{\mathcal{DFD}}} \mathbf{KL}(P(\widetilde{\mathbf{h}}_r|\widetilde{\mathbf{v}}_r) \| P(\widetilde{\mathbf{h}}_s|\widetilde{\mathbf{v}}_s)), \quad (11)$$

where $(\widetilde{\mathbf{v}}_f, \widetilde{\mathbf{v}}_g) \in \widetilde{\mathcal{SFD}}$ and $(\widetilde{\mathbf{v}}_r, \widetilde{\mathbf{v}}_s) \in \widetilde{\mathcal{DFD}}$, $\tilde{\theta} = \{\widetilde{\mathbf{W}}, \widetilde{\mathbf{b}}, \widetilde{\mathbf{c}}\}$ is the parameter of Micro-DGRBM, K_S and K_D are the numbers of two-tuples in $\widetilde{\mathcal{SFD}}$ and $\widetilde{\mathcal{DFD}}$ sets, respectively.

The main goal here is to enhance the representation capabilities of Micro-DRBM and Micro-DGRBM models by fine-tuning the expected representation probability distribution with the stimulation of small disturbance in CD learning process. After running the Markov chain for one step, Eq. (2) can be further transformed to $\mathbf{CD}_1 = \mathbf{KL}(p_0 \| p_\infty) - \mathbf{KL}(p_1 \| p_\infty)$, which has been proven an effective and feasible CD learning method in previous works [34], [33]. Based on the above considerations, the final objective function of the Micro-DRBM model is expressed as

$$\min_{\theta} \left\{ - (1 - \alpha) \left(\mathbf{KL}(p_0 \| p_\infty) - \mathbf{KL}(p_1 \| p_\infty) \right) + \alpha \left[\frac{1}{K_S} \sum_{\mathcal{SFD}} \mathbf{KL}(P(\mathbf{h}_f|\mathbf{v}_f) \| P(\mathbf{h}_g|\mathbf{v}_g)) - \frac{1}{K_D} \sum_{\mathcal{DFD}} \mathbf{KL}(P(\mathbf{h}_r|\mathbf{v}_r) \| P(\mathbf{h}_s|\mathbf{v}_s)) \right] \right\}, \quad (12)$$

where $\alpha \in (0, 1)$ is a scale coefficient. Similarly, the objective function of the Micro-DGRBM model is defined as

$$\min_{\tilde{\theta}} \left\{ - (1 - \alpha) \left(\mathbf{KL}(\tilde{p}_0 \| \tilde{p}_\infty) - \mathbf{KL}(\tilde{p}_1 \| \tilde{p}_\infty) \right) + \alpha \left[\frac{1}{K_S} \sum_{\widetilde{\mathcal{SFD}}} \mathbf{KL}(P(\widetilde{\mathbf{h}}_f|\widetilde{\mathbf{v}}_f) \| P(\widetilde{\mathbf{h}}_g|\widetilde{\mathbf{v}}_g)) - \frac{1}{K_D} \sum_{\widetilde{\mathcal{DFD}}} \mathbf{KL}(P(\widetilde{\mathbf{h}}_r|\widetilde{\mathbf{v}}_r) \| P(\widetilde{\mathbf{h}}_s|\widetilde{\mathbf{v}}_s)) \right] \right\}. \quad (13)$$

Next, we discuss how to solve above two multiobjective optimization problems and obtain the update rules of parameters θ and $\tilde{\theta}$. In Eq. (12), the approximate gradient of $\mathbf{KL}(p_0 \| p_\infty) - \mathbf{KL}(p_1 \| p_\infty)$ with respect to parameters \mathbf{W} , \mathbf{b} and \mathbf{c} can be represented in the following form:

$$-\frac{\partial}{\partial w_{ij}} (\mathbf{KL}(p_0 \| p_\infty) - \mathbf{KL}(p_1 \| p_\infty)) \approx \langle v_i h_j \rangle_0 - \langle v_i h_j \rangle_1, \quad (14)$$

$$-\frac{\partial}{\partial b_j} (\mathbf{KL}(p_0 \| p_\infty) - \mathbf{KL}(p_1 \| p_\infty)) \approx \langle h_j \rangle_0 - \langle h_j \rangle_1 \quad (15)$$

and

$$-\frac{\partial}{\partial c_i} (\mathbf{KL}(p_0 \| p_\infty) - \mathbf{KL}(p_1 \| p_\infty)) \approx \langle v_i \rangle_0 - \langle v_i \rangle_1. \quad (16)$$

Similarly, the approximate gradient of $\mathbf{KL}(\tilde{p}_0 \| \tilde{p}_\infty) - \mathbf{KL}(\tilde{p}_1 \| \tilde{p}_\infty)$ in Eq. (13) with respect to parameters $\widetilde{\mathbf{W}}$, $\widetilde{\mathbf{b}}$ and $\widetilde{\mathbf{c}}$ can be represented in the following form:

$$-\frac{\partial}{\partial \tilde{w}_{ij}} (\mathbf{KL}(\tilde{p}_0 \| \tilde{p}_\infty) - \mathbf{KL}(\tilde{p}_1 \| \tilde{p}_\infty)) \approx \langle \tilde{v}_i \tilde{h}_j \rangle_0 - \langle \tilde{v}_i \tilde{h}_j \rangle_1, \quad (17)$$

$$-\frac{\partial}{\partial \tilde{b}_j} (\mathbf{KL}(\tilde{p}_0 \| \tilde{p}_\infty) - \mathbf{KL}(\tilde{p}_1 \| \tilde{p}_\infty)) \approx \langle \tilde{h}_j \rangle_0 - \langle \tilde{h}_j \rangle_1 \quad (18)$$

and

$$-\frac{\partial}{\partial \tilde{c}_i} (\mathbf{KL}(\tilde{p}_0 \| \tilde{p}_\infty) - \mathbf{KL}(\tilde{p}_1 \| \tilde{p}_\infty)) \approx \langle \tilde{v}_i \rangle_0 - \langle \tilde{v}_i \rangle_1. \quad (19)$$

Then, one of critical tasks is how to obtain the partial derivatives of $\frac{1}{K_S} \sum_{\mathcal{SFD}} \mathbf{KL}(P(\mathbf{h}_f|\mathbf{v}_f) \| P(\mathbf{h}_g|\mathbf{v}_g)) - \frac{1}{K_D} \sum_{\mathcal{DFD}} \mathbf{KL}(P(\mathbf{h}_r|\mathbf{v}_r) \| P(\mathbf{h}_s|\mathbf{v}_s))$ with respect to \mathbf{W} , \mathbf{b} and \mathbf{c} . Another is how to obtain the partial derivatives of $\frac{1}{K_S} \sum_{\widetilde{\mathcal{SFD}}} \mathbf{KL}(P(\widetilde{\mathbf{h}}_f|\widetilde{\mathbf{v}}_f) \| P(\widetilde{\mathbf{h}}_g|\widetilde{\mathbf{v}}_g)) - \frac{1}{K_D} \sum_{\widetilde{\mathcal{DFD}}} \mathbf{KL}(P(\widetilde{\mathbf{h}}_r|\widetilde{\mathbf{v}}_r) \| P(\widetilde{\mathbf{h}}_s|\widetilde{\mathbf{v}}_s))$ with respect to $\widetilde{\mathbf{W}}$, $\widetilde{\mathbf{b}}$ and $\widetilde{\mathbf{c}}$.

Firstly, we rewrite $\mathbf{KL}(P(\mathbf{h}_f|\mathbf{v}_f) \| P(\mathbf{h}_g|\mathbf{v}_g))$ to the following equivalent form:

$$\begin{aligned} & \mathbf{KL}(P(\mathbf{h}_f|\mathbf{v}_f) \| P(\mathbf{h}_g|\mathbf{v}_g)) \\ &= \sum_x p(h_{fx} = 1|\mathbf{v}_f) \log \frac{p(h_{fx} = 1|\mathbf{v}_f)}{p(h_{gx} = 1|\mathbf{v}_g)} \\ &= \sum_x \left[p(h_{fx} = 1|\mathbf{v}_f) \log p(h_{fx} = 1|\mathbf{v}_f) - p(h_{fx} = 1|\mathbf{v}_f) \log p(h_{gx} = 1|\mathbf{v}_g) \right]. \end{aligned} \quad (20)$$

Thus, the gradient of Eq. (20) with respect to weight parameter \mathbf{W} is given by:

$$\begin{aligned} & \frac{\partial}{\partial w_{ij}} \mathbf{KL}(P(\mathbf{h}_f|\mathbf{v}_f) \| P(\mathbf{h}_g|\mathbf{v}_g)) = \\ & \sum_x \left[\frac{\partial}{\partial w_{ij}} p(h_{fx} = 1|\mathbf{v}_f) \log p(h_{fx} = 1|\mathbf{v}_f) + \frac{\partial}{\partial w_{ij}} p(h_{fx} = 1|\mathbf{v}_f) - \frac{\partial}{\partial w_{ij}} p(h_{fx} = 1|\mathbf{v}_f) \log p(h_{gx} = 1|\mathbf{v}_g) - \frac{p(h_{fx} = 1|\mathbf{v}_f) \frac{\partial}{\partial w_{ij}} p(h_{gx} = 1|\mathbf{v}_g)}{p(h_{gx} = 1|\mathbf{v}_g)} \right] \\ &= \sum_x \left\{ \frac{\partial}{\partial w_{ij}} p(h_{fx} = 1|\mathbf{v}_f) \left[\log p(h_{fx} = 1|\mathbf{v}_f) + \log p(h_{gx} = 1|\mathbf{v}_g) + 1 \right] - \frac{p(h_{fx} = 1|\mathbf{v}_f) \frac{\partial}{\partial w_{ij}} p(h_{gx} = 1|\mathbf{v}_g)}{p(h_{gx} = 1|\mathbf{v}_g)} \right\}. \end{aligned} \quad (21)$$

In encoding procedure of Micro-DRBM model, the transformation from the visible layer to the hidden layer is the sigmoid transform. So, the gradient $\frac{\partial}{\partial w_{ij}} p(h_{fx} = 1|\mathbf{v}_f)$ takes the form:

$$\frac{\partial}{\partial w_{ij}} p(h_{fx} = 1|\mathbf{v}_f) = \frac{\partial}{\partial w_{ij}} \sigma(b_x + \sum_i^n v_{fi} w_{ix}). \quad (22)$$

When $x = j$, it is easy to obtain the gradient $\frac{\partial}{\partial w_{ij}} p(h_{fx} = 1 | \mathbf{v}_f) = 1 | \mathbf{v}_f$ as follows.

$$\begin{aligned} \frac{\partial}{\partial w_{ij}} p(h_{fx} = 1 | \mathbf{v}_f) &= \frac{v_{fi} e^{-(b_j + \sum_i^n v_{fi} w_{ij})}}{\left(1 + e^{-(b_j + \sum_i^n v_{fi} w_{ij})}\right)^2} \\ &= h_{fj}(1 - h_{fj})v_{fi}. \end{aligned} \quad (23)$$

In other cases, $\frac{\partial}{\partial w_{ij}} p(h_{fx} = 1 | \mathbf{v}_f) = 0$. Similarly, the gradient $\frac{\partial}{\partial w_{ij}} p(h_{gx} = 1 | \mathbf{v}_g)$ takes the form:

$$\frac{\partial}{\partial w_{ij}} p(h_{gx} = 1 | \mathbf{v}_g) = h_{gj}(1 - h_{gj})v_{gi}. \quad (24)$$

Thus, Eq. (21) can be simplified as the following equivalent form:

$$\begin{aligned} \frac{\partial}{\partial w_{ij}} \mathbf{KL}(P(\mathbf{h}_f | \mathbf{v}_f) \| P(\mathbf{h}_g | \mathbf{v}_g)) \\ = v_{fi} h_{fj}(1 - h_{fj})(\log h_{fj} + \log h_{gj} + 1) - v_{gi} h_{gj}(1 - h_{gj}). \end{aligned} \quad (25)$$

Similarly, the gradient of $\mathbf{KL}(P(\mathbf{h}_r | \mathbf{v}_r) \| P(\mathbf{h}_s | \mathbf{v}_s))$ with respect to weight parameter \mathbf{W} is given by:

$$\begin{aligned} \frac{\partial}{\partial w_{ij}} \mathbf{KL}(P(\mathbf{h}_r | \mathbf{v}_r) \| P(\mathbf{h}_s | \mathbf{v}_s)) \\ = v_{ri} h_{rj}(1 - h_{rj})(\log h_{rj} + \log h_{sj} + 1) - v_{si} h_{sj}(1 - h_{sj}). \end{aligned} \quad (26)$$

From Eqs. (14), (25) and (26), the update rules of \mathbf{W} can be represented in the following form:

$$\begin{aligned} w_{ij}^{(\tau+1)} &= w_{ij}^{(\tau)} + (1 - \alpha)\varepsilon(\langle v_i h_j \rangle_0 - \langle v_i h_j \rangle_1) + \frac{\alpha}{K_S} \sum_{S\mathcal{F}\mathcal{D}} \\ &\left[v_{fi} h_{fj}(1 - h_{fj})(\log h_{fj} + \log h_{gj} + 1) - v_{gi} h_{gj}(1 - h_{gj}) \right] \\ &- \frac{\alpha}{K_D} \sum_{\mathcal{D}\mathcal{F}\mathcal{D}} \left[v_{ri} h_{rj}(1 - h_{rj})(\log h_{rj} + \log h_{sj} + 1) \right. \\ &\left. - v_{si} h_{sj}(1 - h_{sj}) \right], \end{aligned} \quad (27)$$

where ε is a learning rate.

When $x = j$, it is easy to obtain the gradients of $\mathbf{KL}(P(\mathbf{h}_f | \mathbf{v}_f) \| P(\mathbf{h}_g | \mathbf{v}_g))$ and $\mathbf{KL}(P(\mathbf{h}_r | \mathbf{v}_r) \| P(\mathbf{h}_s | \mathbf{v}_s))$ with respect to parameter \mathbf{b} as follows.

$$\begin{aligned} \frac{\partial}{\partial b_j} \mathbf{KL}(P(\mathbf{h}_f | \mathbf{v}_f) \| P(\mathbf{h}_g | \mathbf{v}_g)) \\ = h_{fj}(1 - h_{fj})(\log h_{fj} + \log h_{gj} + 1) - h_{gj}(1 - h_{gj}) \end{aligned} \quad (28)$$

and

$$\begin{aligned} \frac{\partial}{\partial b_j} \mathbf{KL}(P(\mathbf{h}_r | \mathbf{v}_r) \| P(\mathbf{h}_s | \mathbf{v}_s)) \\ = h_{rj}(1 - h_{rj})(\log h_{rj} + \log h_{sj} + 1) - h_{sj}(1 - h_{sj}). \end{aligned} \quad (29)$$

From Eqs. (12), (15), (28) and (29), the update rules of \mathbf{W} can be represented in the following form:

$$\begin{aligned} b_j^{(\tau+1)} &= b_j^{(\tau)} + (1 - \alpha)\varepsilon(\langle h_j \rangle_0 - \langle h_j \rangle_1) + \\ &\frac{\alpha}{K_S} \sum_{S\mathcal{F}\mathcal{D}} [h_{fj}(1 - h_{fj})(\log h_{fj} + \log h_{gj} + 1) - \\ &h_{gj}(1 - h_{gj})] - \frac{\alpha}{K_D} \sum_{\mathcal{D}\mathcal{F}\mathcal{D}} [h_{rj}(1 - h_{rj})(\log h_{rj} + \log h_{sj} \\ &+ 1) - h_{sj}(1 - h_{sj})] \end{aligned} \quad (30)$$

As for model parameter \mathbf{c} , it's obvious that

$$\frac{\partial}{\partial c_i} \mathbf{KL}(P(\mathbf{h}_f | \mathbf{v}_f) \| P(\mathbf{h}_g | \mathbf{v}_g)) = 0 \quad (31)$$

and

$$\frac{\partial}{\partial c_i} \mathbf{KL}(P(\mathbf{h}_r | \mathbf{v}_r) \| P(\mathbf{h}_s | \mathbf{v}_s)) = 0. \quad (32)$$

From Eqs. (16), (31) and (32), the update rule of \mathbf{c} takes the form:

$$c_i^{(\tau+1)} = c_i^{(\tau)} + (1 - \alpha)\varepsilon(\langle v_i \rangle_0 - \langle v_i \rangle_1). \quad (33)$$

Finally, the update rules of \mathbf{W} , \mathbf{b} and \mathbf{c} of the Micro-DRBM model are Eqs. (27), (30) and (33), respectively.

In the Micro-DGRBM model, the hidden units remain binary, but the visible units are the linear units with Gaussian noise. Then, in the encoding process of Micro-DGRBM model, the conditional probability $p(h_j = 1 | \tilde{\mathbf{v}})$ is given by:

$$p(\tilde{h}_j = 1 | \tilde{\mathbf{v}}) = \sigma(\tilde{b}_j + \sum_i \tilde{v}_i \tilde{w}_{ij}) \quad (34)$$

and its conditional probability of reconstructed process takes the form:

$$p(\tilde{\mathbf{v}} | \tilde{\mathbf{h}}) = \mathcal{N}(\sum \tilde{\mathbf{h}} \tilde{\mathbf{W}}^T + \tilde{\mathbf{c}}, \sigma^2). \quad (35)$$

The update rules of the parameters $\tilde{\mathbf{W}}$, $\tilde{\mathbf{b}}$ and $\tilde{\mathbf{c}}$ of the Micro-DGRBM model are similar to the Micro-DRBM model, which takes the form:

$$\begin{aligned} \tilde{w}_{ij}^{(\tau+1)} &= \tilde{w}_{ij}^{(\tau)} + (1 - \alpha)\varepsilon(\langle \tilde{v}_i \tilde{h}_j \rangle_0 - \langle \tilde{v}_i \tilde{h}_j \rangle_1) + \frac{\alpha}{K_S} \sum_{S\mathcal{F}\mathcal{D}} \\ &\left[\tilde{v}_{fi} \tilde{h}_{fj}(1 - \tilde{h}_{fj})(\log \tilde{h}_{fj} + \log \tilde{h}_{gj} + 1) - \tilde{v}_{gi} \tilde{h}_{gj}(1 - \tilde{h}_{gj}) \right] \\ &- \frac{\alpha}{K_D} \sum_{\mathcal{D}\mathcal{F}\mathcal{D}} \left[\tilde{v}_{ri} \tilde{h}_{rj}(1 - \tilde{h}_{rj})(\log \tilde{h}_{rj} + \log \tilde{h}_{sj} + 1) \right. \\ &\left. - \tilde{v}_{si} \tilde{h}_{sj}(1 - \tilde{h}_{sj}) \right], \end{aligned} \quad (36)$$

$$\begin{aligned} \tilde{b}_j^{(\tau+1)} &= \tilde{b}_j^{(\tau)} + (1 - \alpha)\varepsilon(\langle \tilde{h}_j \rangle_0 - \langle \tilde{h}_j \rangle_1) + \\ &\frac{\alpha}{K_S} \sum_{S\mathcal{F}\mathcal{D}} [\tilde{h}_{fj}(1 - \tilde{h}_{fj})(\log \tilde{h}_{fj} + \log \tilde{h}_{gj} + 1) - \\ &\tilde{h}_{gj}(1 - \tilde{h}_{gj})] - \frac{\alpha}{K_D} \sum_{\mathcal{D}\mathcal{F}\mathcal{D}} [\tilde{h}_{rj}(1 - \tilde{h}_{rj})(\log \tilde{h}_{rj} + \log \tilde{h}_{sj} \\ &+ 1) - \tilde{h}_{sj}(1 - \tilde{h}_{sj})] \end{aligned} \quad (37)$$

and

$$\tilde{c}_i^{(\tau+1)} = \tilde{c}_i^{(\tau)} + (1 - \alpha)\varepsilon(\langle \tilde{v}_i \rangle_0 - \langle \tilde{v}_i \rangle_1). \quad (38)$$

3.1.1 Learning Algorithms

In this subsection, we show the learning algorithm of the proposed shallow Micro-DRBM and Micro-DGRBM models according to the update rules of their parameters.

Algorithm 1: Micro-DRBM learning

Input:

$\mathcal{V} = \{\mathbf{v}_1, \mathbf{v}_2, \dots, \mathbf{v}_i, \dots, \mathbf{v}_N\}$: visible layer data;
 $\mathcal{SFD}, \mathcal{DFD}$: Micro-supervised disturbance sets.

Output:

\mathbf{W} , \mathbf{b} and \mathbf{c} : the parameters of Micro-DRBM.

Step 1: Randomly initialize \mathbf{W} , \mathbf{b} and \mathbf{c} .

Step 2: Sample the states of the hidden layer units by $p(h_j = 1|\mathbf{v}) = \sigma(b_j + \sum_i v_i w_{ij})$.

Step 3: Sample the states of the reconstructed visible layer units by $p(v_i = 1|\mathbf{h}) = \sigma(c_i + \sum_j h_j w_{ij})$.

Step 4: Update \mathbf{W} parameter by Eq. (27).

Step 5: Update \mathbf{b} parameter by Eq. (30).

Step 6: Update \mathbf{c} parameter by Eq. (33).

Step 7: **While** iteration less than maximum **go to** Step 2.

step 8: **return** \mathbf{W} , \mathbf{b} and \mathbf{c} .

Algorithm 2: Micro-DGRBM learning

Input:

$\widetilde{\mathcal{V}} = \{\widetilde{\mathbf{v}}_1, \widetilde{\mathbf{v}}_2, \dots, \widetilde{\mathbf{v}}_i, \dots, \widetilde{\mathbf{v}}_N\}$: visible layer data;
 $\widetilde{\mathcal{SFD}}, \widetilde{\mathcal{DFD}}$: Micro-supervised disturbances sets.

Output:

$\widetilde{\mathbf{W}}$, $\widetilde{\mathbf{b}}$ and $\widetilde{\mathbf{c}}$: the parameters of Micro-DGRBM.

Step 1: Randomly initialize $\widetilde{\mathbf{W}}$, $\widetilde{\mathbf{b}}$ and $\widetilde{\mathbf{c}}$.

Step 2: Sample the states of the hidden layer units by $p(\widetilde{h}_j = 1|\widetilde{\mathbf{v}}) = \sigma(\widetilde{b}_j + \sum_i \widetilde{v}_i \widetilde{w}_{ij})$.

Step 3: Sample the states of the reconstructed visible layer units by $p(\widetilde{\mathbf{v}}|\widetilde{\mathbf{h}}) = \mathcal{N}(\sum \widetilde{\mathbf{h}} \widetilde{\mathbf{W}}^T + \widetilde{\mathbf{c}}, \sigma^2)$.

Step 4: Update $\widetilde{\mathbf{W}}$ parameter by Eq. (36).

Step 5: Update $\widetilde{\mathbf{b}}$ parameter by Eq. (37).

Step 6: Update $\widetilde{\mathbf{c}}$ parameter by Eq. (38).

Step 7: **While** iteration less than maximum **go to** Step 2.

step 8: **return** $\widetilde{\mathbf{W}}$, $\widetilde{\mathbf{b}}$ and $\widetilde{\mathbf{c}}$.

3.2 Micro-DL Architecture

In the proposed shallow Micro-DGRBM and Micro-DRBM models, the small-perturbation ideology is firstly introduced on the representation learning model based on the representation probability distribution. The positive SPI is used to stimulate the representation learning process from the perspective of representation probability distribution. To explore the representation learning capability under the continuous stimulation of small disturbance, we present a deep Micro-DL framework based on the Micro-DGRBM and Micro-DRBM models in this section. The deep Micro-DL framework consists of a stack of one Micro-DGRBM and N Micro-DRBMs to explore superior performances for modeling continuous data. In the proposed deep architecture, the visible layer consists of Gaussian linear units and all hidden

layers consist of binary units. In the process of CD learning of shallow Micro-DGRBM model, the SPI is used as small positive disturbance in the encoding and reconstruction procedures which adopt the binary and linear transformation by 1 step Gibbs sampling, respectively. However, the SPI is used as small positive disturbance in the encoding and reconstruction procedures which all adopt the binary transformation by 1 step Gibbs sampling in the process of CD learning of shallow Micro-DRBM model.

The architecture of the proposed Micro-DL is shown in Fig. 1. The hidden feature vector of Micro-DGRBM model, $\mathbf{h}_{(1)}$, is the input of the next Micro-DRBM model. And the hidden feature vector of this Micro-DRBM model, $\mathbf{h}_{(2)}$, is the input of its next Micro-DRBM model. The final hidden feature vector of our Micro-DL architecture, $\mathbf{h}_{(N)}$, is the input of the following clustering task. In the stack of Micro-DRBMs, $\mathbf{h}'_{(i)}$ is the reconstructed vector.

In order to prove the effectiveness of the continuous stimulation of small disturbance, we design a most related deep representation learning framework, None Micro-supervised Disturbance Learning (NMicro-DL), which consists of one traditional shallow GRBM and N RBM models. The only difference between Micro-DL and NMicro-DL architectures is that the continuous stimulation of small disturbance is used to fine-tune the expected representation distribution in the CD learning process of the former and the latter is an unsupervised deep representation learning framework.

4 EXPERIMENTS

In this section, we compare the performance of the proposed Micro-DL with deep unsupervised learning models, shallow and deep semi-supervised learning models. All experiments have been conducted clustering tasks on twelve datasets. The details of experimental datasets are as follows:

- Microsoft Research Asia Multimedia image sub-dataset (MSRA-MM) [49]: Aquarium (922 images, 892 features and 3 classes), bathroom (924 images, 892 features and 3 classes), blog (943 images, 892 features and 3 classes), blood (866 images, 892 features and 3 classes), bouquet (880 images, 892 features and 3 classes), bugat (882 images, 892 features and 3 classes), cactus (919 images, 892 features and 3 classes), voituretuning (799 images, 899 features and 3 classes).
- car¹: This UCI dataset is derived from simple hierarchical decision mode, which contains 1728 instances, 6 features and 4 classes.
- KDD99²: We choose 5904 instances from a large-scale dataset (KDD Cup 1999, 4000000 instances) randomly. It comprises 41 features and 3 classes.
- segmentation³: This image segmentation dataset contains 2100 instances, 19 features and 7 classes.
- vowe⁴: This dataset contains information about speaker independent recognition which is a merge of the two original databases preset at the UCI repository⁵. It has 990 instances, 13 features and 11 classes.

1. <https://archive.ics.uci.edu/ml/datasets/car+evaluation>
2. <https://archive.ics.uci.edu/ml/datasets/kdd+cup+1999+data>
3. <http://archive.ics.uci.edu/ml/support/image+segmentation>
4. <https://sci2s.ugr.es/keel/dataset.php?cod=113>
5. <http://archive.ics.uci.edu/ml/datasets.php>

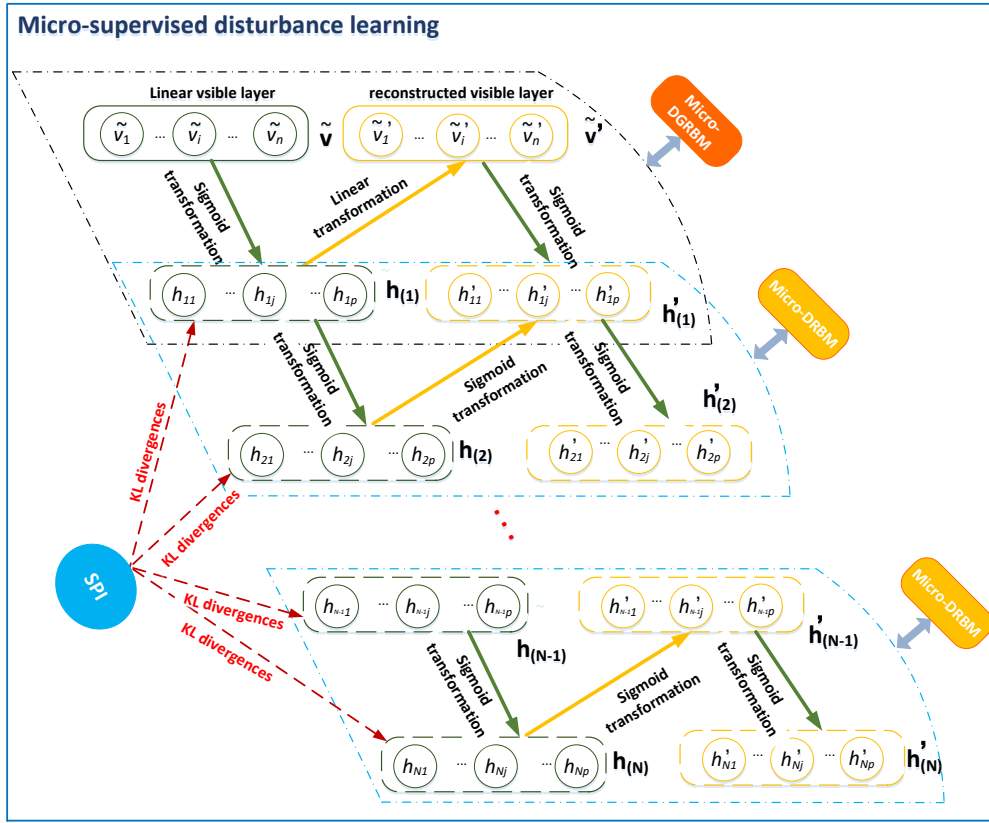


Fig. 1: The deep Micro-DL architecture consists of a stack of one shallow Micro-DGRBM and $N - 1$ shallow Micro-DRBMs. It has one Gaussian linear visible layer and N binary hidden layers. The SPI is used to explore the representation learning capability of Micro-DL under the continuous stimulation of small disturbance.

In order to evaluate the representation capability of the proposed Micro-DL architecture, we compare the clustering performance of our Micro-DL against Semi-SP [50], VGAE [13], None Micro-DL (NMicro-DL), pcGRBM [34], Semi-EAGR [51] and Semi-MG [32]. For all contrastive shallow models (pcGRBM and Semi-EAGR) and deep frameworks (VGAE, NMicro-DL and Semi-MG), the performance evaluations have two stages: one is feature learning and the other is clustering analysis. The output features of them are the input of Spectral Clustering [52] algorithm.

In the representation learning process of our Micro-DL and NMicro-DL architectures, the dimension of the hidden layer is the same as the visible layer. For the first group datasets (MSRA-MM), the Micro-DL architecture consists of one Micro-DGRBM and sixteen Micro-DRBMs. To compare fairness, the learning rates of our Micro-DL architecture are the same as NMicro-DL model for training MSRA-MM datasets. Both of them are 10^{-4} . For the second group datasets (UCI), the Micro-DL architecture consists of six hidden layers. The learning rates of the weights, biases of visible and hidden layers of Micro-DGRBM and Micro-DRBM models are set to 10^{-8} . In our Micro-DL architecture, the scale coefficient of Micro-DGRBM and Micro-DRBM are set to 0.3 for all twelve datasets. The number of hidden layer units of Micro-DL is 892 on the aquarium, bathroom, blog, blood, bouquet, bugat and cactus datasets. They are 899, 6, 41, 19 and 13 on the voituretuning, car, KDD99, segmentation and vowe datasets, respectively.

4.1 Evaluation Metrics

Four popular external evaluation metrics that are used in the paper to assess the experimental results are the clustering accuracy [53], Jaccard index (Jac index) [54], Fowlkes and Mallows index (FM index) [55] and Rand index [56]. Furthermore, the Friedman aligned ranks test [57]) is used to provide fair comparisons among different methods. The calculations of four external metrics are provided as follows:

- 1) The clustering accuracy metric is used to calculate the ratio of the instance assigned to the correct clusters. It is defined to be

$$accuracy = \frac{\sum_{i=1}^N F(l_i, l'_i)}{N}, \quad (39)$$

where N is the number of instances, l_i and l'_i are the target and predicted label of the i th instance, respectively. If $l_i = l'_i$, then $F(l_i, l'_i) = 1$. Otherwise, $F(l_i, l'_i) = 0$.

- 2) The Jaccard Index measures similarity between sample sets can be written as

$$Jac = \frac{|A \cap B|}{|A \cup B|}, \quad (40)$$

where A and B are finite sample sets.

- 3) The Fowlkes and Mallows index calculates the similarity between the benchmark classifications and the clusters returned by the clustering algorithm. It is defined as

$$FMI = \sqrt{\frac{TP}{TP + FP} \times \frac{TP}{TP + FN}}, \quad (41)$$

where TP , FP and FN are the numbers of true positives, false positives and false negatives, respectively.

- 4) The Rand index is a measure of the percentage of correct decisions made by the algorithm. It is defined to be

$$Rand = \frac{TP + TN}{TP + FP + FN + TN}, \quad (42)$$

where TN is the number of true negatives.

The Friedman aligned ranks test is an advanced and popular nonparametric test method which can be used to analyze the performance of algorithms. It can be written as

$$T = \frac{(n-1)(\sum_{j=1}^n \hat{r}_{.j}^2 - nm^2(nm+1)^2/4)}{nm(nm+1)(2nm+1)/6 - \sum_{i=1}^m \hat{r}_{i.}^2/n}, \quad (43)$$

where $\hat{r}_{.j}$ is the total ranks of the j th data set, $\hat{r}_{i.}$ is the total ranks of the i th algorithm, n is the number of algorithm and m is the number of data set. The test statistic T is compared for significance with a chi-square distribution for $n-1$ degrees of freedom.

4.2 Clustering Performance

We first compare the proposed Micro-DL architecture with benchmarking algorithm (Semi-SP). To prove deep representation learning capability of our Micro-DL, we compare it with the most related shallow semi-supervised feature learning models (pcGRBM [34] and Semi-EAGR [51]). Then, two unsupervised deep representation models (VGAE and NMicro-DL) are compared with our Micro-DL model to show the effectiveness of the proposed Micro-supervised strategy. Significantly, the NMicro-DL is the most related deep learning model with our Micro-DL architecture. Hence, we compare the performance of them to evaluate that the distributions of deep hidden features of our Micro-DL are whether or not more reasonable than the NMicro-DL model. Finally, we compare further the proposed Micro-DL architecture with deep semi-supervised model (Semi-MG [32]) to evaluate impartially the capability of deep representation learning.

All results of clustering accuracy are listed in Table 1. On the whole, the average clustering accuracies of Semi-SP, pcGRBM, Semi-EAGR, Semi-MG, VGAE and NMicro-DL are 0.3724, 0.4335, 0.4656, 0.6692, 0.5789, 0.5619, respectively. However, the clustering accuracy of our Micro-DL architecture increases to 0.7343. It's obvious that the performance of the Micro-DL is significantly increased by 0.3619 when it is compared with the Semi-SP algorithm. These results demonstrates that its output features have reasonable distributions than visible layer data for clustering. In contrast to the pcGRBM and Semi-EAGR models, the performances of the proposed Micro-DL framework are increased by 0.3018 and 0.2687, respectively. Thus, the results indicate that the capability of deep representation learning of our Micro-DL is more powerful than shallow representation learning of the most related contrastive models. When the proposed Micro-DL

architecture is compared with the Semi-MG, VGAE and NMicro-DL, the performances are increased by 0.0651, 0.1554 and 0.1724, respectively. Hence, we can conclude that the distributions of hidden layers of our Micro-DL are more reasonable under the stimulation of the SPI than all contrast deep models.

As shown in Table 2, the average Jac of Semi-SP, pcGRBM, Semi-EAGR, Semi-MG, VGAE and NMicro-DL are 0.2521, 0.3123, 0.3224, 0.5073, 0.4148 and 0.4015, respectively. However, our Micro-DL architecture raises the Jac metric to 0.5836 significantly. In contrast to the Semi-SP algorithm, it improves the performance by 0.3315. These results demonstrates again that the hidden features of the Micro-DL architecture have reasonable distributions than visible layer data for clustering. The Jac indices of Micro-DL are increased by 0.2713 and 0.2612 when it is compared with the pcGRBM and Semi-EAGR models, respectively. Furthermore, in contrast to Semi-MG, VGAE and NMicro-DL frameworks, our Micro-DL improves the Jac by 0.0763, 0.1688 and 0.1821, respectively. Hence, these results illustrate that the proposed Micro-DL has more outstanding capability of deep representation learning under the stimulation of the SPI than contrast shallow models and deep frameworks.

In Table 3, the average FMs of Semi-SP, pcGRBM, Semi-EAGR, Semi-MG, VGAE and NMicro-DL are 0.4077, 0.4710, 0.4935, 0.6807, 0.5913 and 0.5665, respectively. However, the average FM index of our Micro-DL architecture is raised to 0.7564 significantly. In contrast to the Semi-SP algorithm, it improves the performance by 0.3487. When the proposed Micro-DL is compared with the pcGRBM and Semi-EAGR models, the FM indices are increased by 0.2854 and 0.2629, respectively. Furthermore, in contrast to Semi-MG, VGAE and NMicro-DL frameworks, our Micro-DL architecture improves the FM by 0.0757, 0.1651 and 0.1899, respectively. Hence, these comparisons show that our Micro-DL has exciting capability of deep representation learning for clustering.

The results of Rand index are presented in Table 4. The average Rand of Semi-SP, pcGRBM, Semi-EAGR, Semi-MG, VGAE and NMicro-DL are 0.5085, 0.5508, 0.5285, 0.5639, 0.5264 and 0.5408, respectively. However, the proposed Micro-DL raises the average Rand to 0.5988. In contrast to the Semi-SP algorithms, it improves the metric of average Rand by 0.0903. The average Rand indices of our Micro-DL are increased by 0.0480 and 0.0703 when it is compared with the pcGRBM and Semi-EAGR models, respectively. Furthermore, in contrast to Semi-MG, VGAE and NMicro-DL frameworks, our Micro-DL improves the metric of average Rand by 0.0349, 0.0724 and 0.0580, respectively.

Fig. 2 presents visual contrast of the clustering performances (accuracy, Jac, FM and Rand) among the benchmarking algorithms, shallow models and deep frameworks on twelve datasets. On the whole, we can see that our Micro-DL architecture shows fairly competitive performances in all evaluation metrics.

4.3 Friedman Aligned Ranks Test

In the experiments, the Friedman Aligned Ranks test is based on 12 datasets and 7 contrast algorithms of ranks. The average ranks provide a fair comparison of these algorithms. On average, the proposed Micro-DL ranks the first with the value of 9.4167; the Semi-MG, VGAE and NMicro-DL ranks the second, third and fourth, with the values of 25.2500, 38.1667 and 42.0833, respectively; and the fifth, sixth and the last are the Semi-EAGR, pcGRBM and Semi-SP with ranks 56.5833, 59.4167 and 66.5833, respectively.

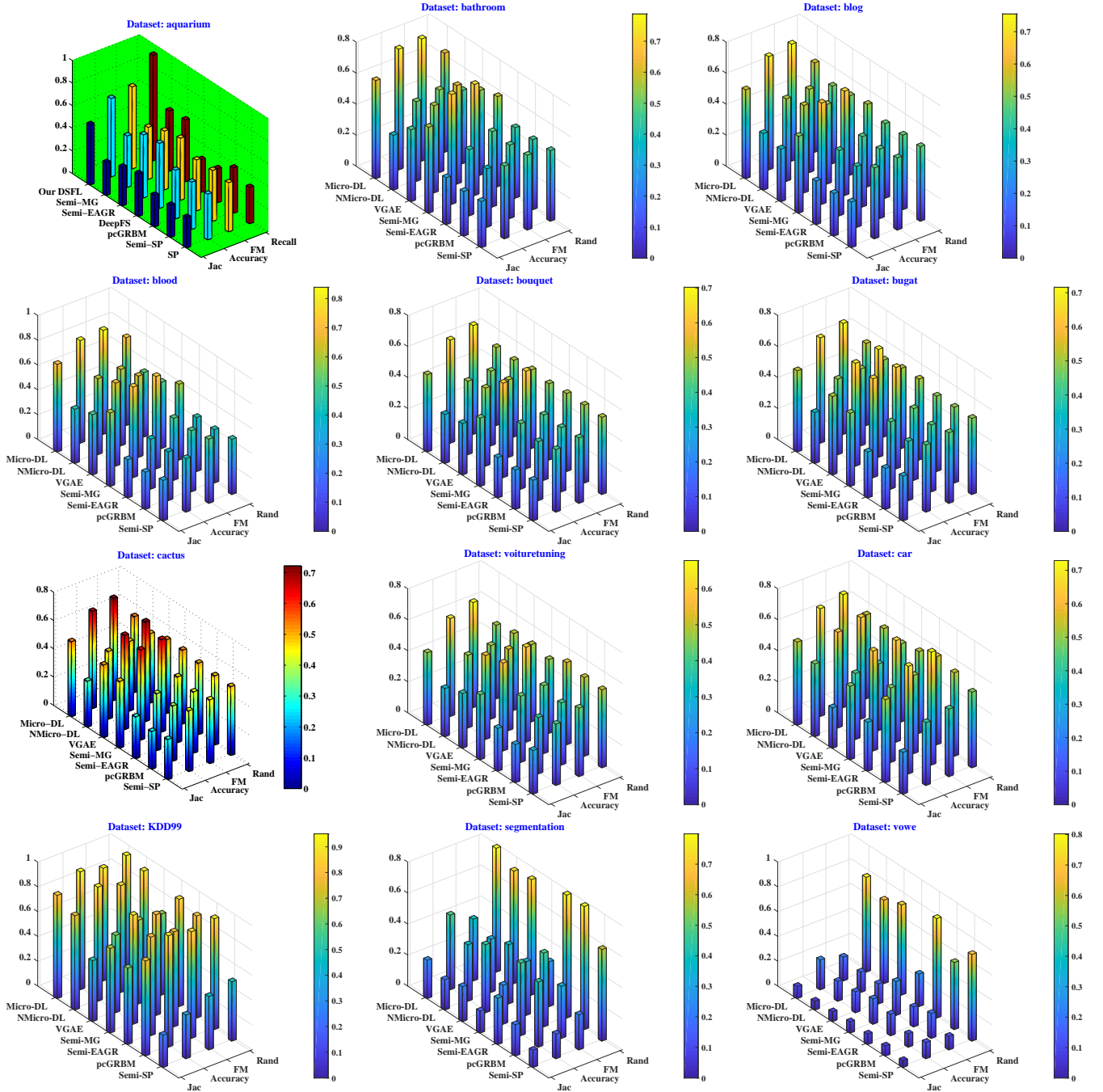


Fig. 2: Performance comparisons (Accuracy, Jac index, FM index and Rand index) of benchmarking algorithms (Semi-SP), shallow models (pcGRBM and Semi-EAGR), and deep models (Semi-MG, VGAE, NMicro-DL and Micro-DL).

Under the null hypothesis, the Friedman Aligned Ranks test is used to check whether the metrical sum of aligned ranks are different from the average of total aligned rank $\widehat{R}_j = 510$:

$$\begin{aligned} & \sum_{j=1}^k \widehat{R}_{\cdot,j}^2 \\ &= 799^2 + 713^2 + 679^2 + 303^2 + 458^2 + 505^2 + 113^2 \\ &= 2177178, \end{aligned} \quad (44)$$

$$\begin{aligned} \sum_{j=1}^k \widehat{R}_{i,\cdot}^2 &= 304^2 + 303^2 + 300^2 + 312^2 + 294^2 + 298^2 + 302^2 \\ &\quad + 299^2 + 303^2 + 256^2 + 302^2 + 297^2 = 1064172, \end{aligned} \quad (45)$$

$$\begin{aligned} T &= \frac{(7-1)(2177178 - 7 \cdot 12^2(7 \cdot 12 + 1)^2/4)}{7 \cdot 12(7 \cdot 12 + 1)(2 \cdot 7 \cdot 12 + 1)/6 - 1064172/7} \\ &= 43.5744, \end{aligned} \quad (46)$$

With seven algorithms and 12 data sets, T is a chi-square distribution with six degree-of-freedom. The null hypothesis is rejected because the p -value of T is 1×10^{-8} which is far less than 0.05.

TABLE 1: Performance comparisons (Accuracy) of benchmarking algorithms (Semi-SP), shallow models (pcGRBM and Semi-EAGR), and deep models (Semi-MG, VGAE, NMicro-DL and Micro-DL). The larger clustering accuracy, the better performance. The best performance on each data set is bolded.

Dataset	Semi-SP	pcGRBM	Semi-EAGR	Semi-MG	VGAE	NMicro-DL	Micro-DL
aquarium	0.4242 ± 0.0489	0.4030 ± 0.0104	0.4421 ± 0.0178	0.6245 ± 0.0556	0.5701 ± 0.0455	0.5157 ± 0.0328	0.6943 ± 0.0047
bathroom	0.4695 ± 0.0610	0.3774 ± 0.0106	0.4268 ± 0.0291	0.7083 ± 0.0651	0.5624 ± 0.0579	0.5141 ± 0.0293	0.7792 ± 0.0053
blog	0.4575 ± 0.0319	0.3930 ± 0.0092	0.4221 ± 0.0197	0.6538 ± 0.0588	0.5637 ± 0.0739	0.5323 ± 0.0491	0.7314 ± 0.0048
blood	0.4309 ± 0.0580	0.3931 ± 0.0111	0.4030 ± 0.0157	0.7304 ± 0.0738	0.6697 ± 0.0358	0.6125 ± 0.0158	0.8279 ± 0.0057
bouquet	0.4035 ± 0.0439	0.3803 ± 0.0133	0.4224 ± 0.0231	0.6093 ± 0.0439	0.5034 ± 0.0658	0.4735 ± 0.0328	0.6653 ± 0.0045
bugat	0.4334 ± 0.0378	0.3825 ± 0.0138	0.4336 ± 0.0201	0.6381 ± 0.0428	0.6636 ± 0.0055	0.4870 ± 0.0457	0.6795 ± 0.0045
cactus	0.4294 ± 0.0440	0.3898 ± 0.0127	0.4033 ± 0.0181	0.6381 ± 0.0428	0.6664 ± 0.0047	0.4785 ± 0.0353	0.6878 ± 0.0046
voituretuning	0.3949 ± 0.0390	0.3634 ± 0.0154	0.4272 ± 0.0312	0.5668 ± 0.0383	0.5414 ± 0.0314	0.4686 ± 0.0310	0.6318 ± 0.0042
car	0.4051 ± 0.0641	0.6941 ± 0.0143	0.4800 ± 0.0331	0.6444 ± 0.0398	0.4251 ± 0.0551	0.6170 ± 0.0145	0.6948 ± 0.0024
KDD99	0.3519 ± 0.0077	0.8983 ± 0.1049	0.7950 ± 0.0941	0.8784 ± 0.0190	0.6231 ± 0.0222	0.9199 ± 0.0222	0.9505 ± 0.0001
segmentation	0.1587 ± 0.0041	0.4196 ± 0.0520	0.4688 ± 0.0579	0.2514 ± 0.0779	0.4383 ± 0.0756	0.3643 ± 0.0111	0.4814 ± 0.0101
vowe	0.1309 ± 0.0042	0.1079 ± 0.0073	0.1737 ± 0.0110	0.2037 ± 0.0817	0.1691 ± 0.0147	0.1601 ± 0.0179	0.2404 ± 0.0286
Average	0.3742	0.4335	0.4656	0.6692	0.5789	0.5619	0.7343

TABLE 2: Performance comparisons (Jac index) of benchmarking algorithms (Semi-SP), shallow models (pcGRBM and Semi-EAGR), and deep models (Semi-MG, VGAE, NMicro-DL and Micro-DL). The larger Jac, the better performance. The best performance on each data set is bolded.

Dataset	Semi-SP	pcGRBM	Semi-EAGR	Semi-MG	VGAE	NMicro-DL	Micro-DL
aquarium	0.2906 ± 0.0047	0.2672 ± 0.0015	0.2715 ± 0.0041	0.4708 ± 0.0477	0.4026 ± 0.0032	0.3461 ± 0.0216	0.5343 ± 0.0024
bathroom	0.2975 ± 0.0035	0.2885 ± 0.0016	0.3029 ± 0.0216	0.5540 ± 0.0692	0.4641 ± 0.0520	0.3542 ± 0.0215	0.6327 ± 0.0190
blog	0.2940 ± 0.0055	0.2755 ± 0.0016	0.2816 ± 0.0112	0.4957 ± 0.0547	0.3398 ± 0.0686	0.3662 ± 0.0342	0.5733 ± 0.0028
blood	0.3271 ± 0.0314	0.3005 ± 0.0019	0.3082 ± 0.0161	0.5924 ± 0.0805	0.4858 ± 0.0709	0.4370 ± 0.0140	0.7067 ± 0.0051
bouquet	0.2622 ± 0.0100	0.2546 ± 0.0022	0.2606 ± 0.0065	0.4408 ± 0.0421	0.3322 ± 0.0757	0.3166 ± 0.0173	0.4983 ± 0.0017
bugat	0.2889 ± 0.0145	0.2654 ± 0.0022	0.2964 ± 0.0240	0.4722 ± 0.0474	0.5060 ± 0.0789	0.3285 ± 0.0286	0.5239 ± 0.0032
cactus	0.2842 ± 0.0162	0.2660 ± 0.0026	0.2954 ± 0.0309	0.4722 ± 0.0474	0.5138 ± 0.0799	0.3253 ± 0.0209	0.5306 ± 0.0056
voituretuning	0.2822 ± 0.0136	0.2463 ± 0.0026	0.2763 ± 0.0225	0.4192 ± 0.0374	0.3529 ± 0.0838	0.3111 ± 0.0186	0.4676 ± 0.0032
car	0.2701 ± 0.0428	0.5356 ± 0.0160	0.3158 ± 0.0227	0.4738 ± 0.0455	0.2608 ± 0.0923	0.4701 ± 0.1197	0.5365 ± 0.0026
KDD99	0.2605 ± 0.0382	0.7663 ± 0.1737	0.6153 ± 0.0007	0.6818 ± 0.0288	0.4903 ± 0.0991	0.7603 ± 0.1076	0.8326 ± 0.0008
segmentation	0.1115 ± 0.0123	0.2015 ± 0.0308	0.2986 ± 0.0023	0.1414 ± 0.0014	0.2250 ± 0.0462	0.1957 ± 0.0231	0.2469 ± 0.0569
vowe	0.0561 ± 0.0051	0.0806 ± 0.0023	0.0846 ± 0.0087	0.0903 ± 0.0014	0.0784 ± 0.0076	0.0715 ± 0.0248	0.0980 ± 0.0093
Average	0.2521	0.3123	0.3224	0.5073	0.4148	0.4015	0.5836

TABLE 3: Performance comparisons (FM index) of benchmarking algorithms (Semi-SP), shallow models (pcGRBM and Semi-EAGR), and deep models (Semi-MG, VGAE, NMicro-DL and Micro-DL). The larger FM, the better performance. The best performance on each data set is bolded.

Dataset	Semi-SP	pcGRBM	Semi-EAGR	Semi-MG	VGAE	NMicro-DL	Micro-DL
aquarium	0.4565 ± 0.0047	0.4333 ± 0.0019	0.4392 ± 0.0052	0.6545 ± 0.0545	0.5790 ± 0.0035	0.5151 ± 0.0227	0.7266 ± 0.0026
bathroom	0.4822 ± 0.0028	0.4737 ± 0.0020	0.4860 ± 0.0204	0.7166 ± 0.0632	0.6353 ± 0.0466	0.5329 ± 0.0200	0.7878 ± 0.0174
blog	0.4654 ± 0.0063	0.4481 ± 0.0019	0.4538 ± 0.0127	0.6731 ± 0.0581	0.5137 ± 0.0663	0.5376 ± 0.0344	0.7545 ± 0.0027
blood	0.5173 ± 0.0282	0.4931 ± 0.0017	0.5005 ± 0.0146	0.7448 ± 0.0672	0.6551 ± 0.0679	0.6166 ± 0.0117	0.8387 ± 0.0039
bouquet	0.4219 ± 0.0110	0.4146 ± 0.0029	0.4213 ± 0.0080	0.6299 ± 0.0532	0.4990 ± 0.0753	0.4813 ± 0.0194	0.7021 ± 0.0015
bugat	0.4555 ± 0.0149	0.4313 ± 0.0027	0.4627 ± 0.0245	0.6540 ± 0.0549	0.6961 ± 0.0823	0.4964 ± 0.0303	0.7158 ± 0.0036
cactus	0.4501 ± 0.0164	0.4321 ± 0.0028	0.4643 ± 0.0330	0.6540 ± 0.0549	0.7049 ± 0.0853	0.4929 ± 0.0218	0.7222 ± 0.0052
voituretuning	0.4415 ± 0.0152	0.4012 ± 0.0032	0.4378 ± 0.0249	0.6125 ± 0.0509	0.5246 ± 0.0903	0.4748 ± 0.0219	0.6783 ± 0.0032
car	0.4355 ± 0.0450	0.7287 ± 0.0186	0.5043 ± 0.0247	0.6553 ± 0.0533	0.4304 ± 0.0987	0.6551 ± 0.1312	0.7289 ± 0.0029
KDD99	0.4308 ± 0.0669	0.8594 ± 0.1151	0.7653 ± 0.0004	0.8119 ± 0.0198	0.6750 ± 0.1028	0.8617 ± 0.0696	0.9086 ± 0.0005
segmentation	0.2261 ± 0.0430	0.3357 ± 0.0425	0.4758 ± 0.0019	0.3458 ± 0.0196	0.3813 ± 0.0619	0.3426 ± 0.0198	0.3982 ± 0.0692
vowe	0.1091 ± 0.0134	0.2003 ± 0.0161	0.1603 ± 0.0163	0.2732 ± 0.0170	0.1625 ± 0.0238	0.1644 ± 0.0877	0.1920 ± 0.0098
Average	0.4077	0.4710	0.4935	0.6807	0.5913	0.5665	0.7564

Therefore, we can conclude that these algorithms are significantly different.

4.4 Friedman + Post-hoc Nemenyi Tests

The results of Friedman + pos-hoc Nemenyi tests [58] among all contrastive methods are shown in Fig. 3. Besides the results of Micro-DL versus Semi-MG, most of the test results between Micro-DL framework and other contrastive methods are less than 0.05. Hence, Friedman + pos-hoc Nemenyi tests confirm the striking differences between Micro-DL framework and most other contrastive methods at the significance level (5%). Furthermore, the result of Friedman + pos-hoc Nemenyi tests between Micro-

DL and NMicro-DL is 0.0023 which is far below 0.05. So, there is striking difference between the Micro-DL and NMicro-DL frameworks under the stimulation of SPI in the former. In fact, the results of Micro-DL versus Semi-SP and Micro-DL versus pcGRBM are approximately 3×10^{-7} , which are far less than 0.05. It's obvious that there are significant difference between Micro-DL versus Semi-SP and pcGRBM.

4.5 Effectiveness of the SPI

To prove the effectiveness of SPI in the Micro-DL architecture, we compare the performance of our Micro-DL architecture with NMicro-DL which is a most related unsupervised deep repre-

TABLE 4: Performance comparisons (Rand index) of benchmarking algorithms (Semi-SP), shallow models (pcGRBM and Semi-EAGR), and deep models (Semi-MG, VGAE, NMicro-DL and Micro-DL). The larger recall, the better performance. The best performance on each data set is bolded.

Dataset	Semi-SP	pcGRBM	Semi-EAGR	Semi-MG	VGAE	NMicro-DL	Micro-DL
aquarium	0.4864 ± 0.0007	0.4892 ± 0.0018	0.4955 ± 0.0047	0.5100 ± 0.0187	0.4677 ± 0.0028	0.5005 ± 0.0077	0.5388 ± 0.0033
bathroom	0.4555 ± 0.0001	0.4517 ± 0.0017	0.4548 ± 0.0099	0.5813 ± 0.0478	0.5462 ± 0.0480	0.4731 ± 0.0099	0.6395 ± 0.0141
blog	0.4812 ± 0.0043	0.4812 ± 0.0013	0.4817 ± 0.0088	0.5315 ± 0.0277	0.5134 ± 0.0408	0.5008 ± 0.0103	0.5768 ± 0.0029
blood	0.4451 ± 0.0163	0.4304 ± 0.0011	0.4354 ± 0.0084	0.6108 ± 0.0661	0.5346 ± 0.0376	0.5196 ± 0.0088	0.7084 ± 0.0051
bouquet	0.4980 ± 0.0005	0.5022 ± 0.0026	0.5035 ± 0.0057	0.4922 ± 0.0058	0.5076 ± 0.0338	0.4951 ± 0.0062	0.5032 ± 0.0033
bugat	0.4909 ± 0.0014	0.4887 ± 0.0025	0.4865 ± 0.0073	0.5224 ± 0.0109	0.5177 ± 0.0307	0.4968 ± 0.0104	0.5300 ± 0.0025
cactus	0.4873 ± 0.0002	0.4894 ± 0.0018	0.5043 ± 0.0138	0.5224 ± 0.0109	0.5224 ± 0.0285	0.4915 ± 0.0051	0.5372 ± 0.0065
voituretuning	0.5030 ± 0.0060	0.5084 ± 0.0014	0.5305 ± 0.0064	0.4759 ± 0.0062	0.4976 ± 0.0274	0.4958 ± 0.0076	0.4747 ± 0.0041
car	0.4876 ± 0.0075	0.5390 ± 0.0074	0.5689 ± 0.0151	0.5274 ± 0.0073	0.5036 ± 0.0273	0.5274 ± 0.0246	0.5410 ± 0.0025
KDD99	0.4776 ± 0.0584	0.8940 ± 0.0956	0.8237 ± 0.0006	0.8653 ± 0.0164	0.6528 ± 0.0774	0.9072 ± 0.0466	0.9389 ± 0.0003
segmentation	0.5909 ± 0.1082	0.7942 ± 0.0166	0.7933 ± 0.0094	0.2892 ± 0.1028	0.7447 ± 0.0456	0.7256 ± 0.0634	0.7991 ± 0.0455
vowe	0.6979 ± 0.0301	0.5407 ± 0.0612	0.8024 ± 0.0091	0.2619 ± 0.1206	0.7266 ± 0.0514	0.6729 ± 0.2284	0.7644 ± 0.0352
Average	0.5085	0.5508	0.5285	0.5639	0.5264	0.5408	0.5988

TABLE 5: Performance comparisons (Rank) of benchmarking algorithms (Semi-SP), shallow models (pcGRBM and Semi-EAGR), and deep models (Semi-MG, VGAE, NMicro-DL and Micro-DL). The smaller rank, the better performance.

Dataset	Semi-SP	pcGRBM	Semi-EAGR	Semi-MG	VGAE	NMicro-DL	Micro-DL	Total
aquarium	-0.1006 (65)	-0.1218 (71)	-0.0827 (58)	0.0997 (25)	0.0453 (34)	-0.0091 (45)	0.1695 (6)	304
bathroom	-0.0787 (56)	-0.1708 (80)	-0.1214 (69)	0.1601 (8)	0.0142 (39)	-0.0341 (49)	0.2310 (2)	303
blog	-0.0788 (57)	-0.1433 (75)	-0.1142 (67)	0.1175 (18)	0.0274 (37)	-0.0040 (43)	0.1951 (3)	300
blood	-0.1502 (77)	-0.1880 (82)	-0.1781 (81)	0.1493 (9)	0.0886 (26)	0.0314 (36)	0.2468 (1)	312
bouquet	-0.0905 (61)	-0.1137 (66)	-0.0716 (55)	0.1153 (19)	0.0094 (40)	-0.0205 (48)	0.1713 (5)	294
bugat	-0.0977 (63)	-0.1486 (76)	-0.0975 (62)	0.1070 (22)	0.1325 (14)	-0.0441 (51)	0.1484 (10)	298
cactus	-0.0982 (64)	-0.1378 (73)	-0.1243 (72)	0.1105 (21)	0.1388 (13)	-0.0491 (52)	0.1602 (7)	302
voituretuning	-0.0900 (60)	-0.1215 (70)	-0.0577 (53)	0.0819 (27)	0.0565 (31)	-0.0163 (47)	0.1469 (11)	299
car	-0.1607 (79)	0.1283 (16)	-0.0858 (59)	0.0786 (28)	-0.1407 (74)	0.0512 (32)	0.1290 (15)	303
KDD99	-0.4220 (84)	0.1244 (17)	0.0211 (38)	0.1045 (23)	-0.1508 (78)	0.1460 (12)	0.1766 (4)	256
segmentation	-0.2102 (83)	0.0507 (33)	0.0999 (24)	-0.1175 (68)	0.0694 (30)	-0.0046 (44)	0.1125 (20)	302
vowe	-0.0385 (50)	-0.0615 (54)	0.0043 (41)	0.0343 (35)	-0.0003 (42)	-0.0093 (46)	0.0710 (29)	297
Total	799	713	679	303	458	505	113	3570
Average Rank	66.5833	59.4167	56.5833	25.2500	38.1667	42.0833	9.4167	

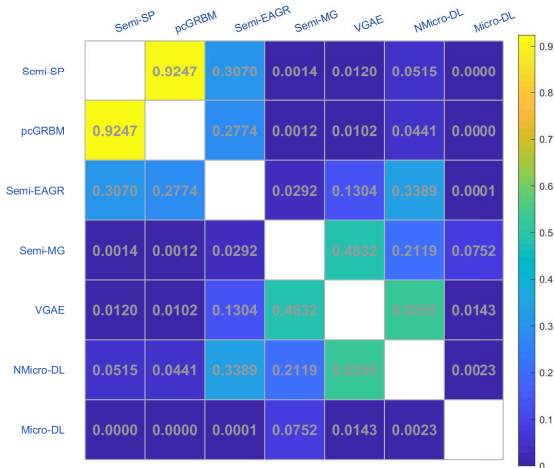


Fig. 3: The results of Friedman + post-hoc Nemenyi tests among all contrastive algorithms.

sentation learning framework. The results are shown in Fig. 4. It is obvious that the proposed Micro-DL architecture shows higher performances than NMicro-DL framework for clustering. Although the depth structures of Micro-DL and NMicro-DL are almost identical, the representation learning capability is improved by constantly stimulating the representation probability distribu-

tion with the SPI.

4.6 Sensibility of the Scale Coefficient

To show the sensibility of the scale coefficient α , we gradually increase it from 0.1 to 0.9 with 0.1 per step in the learning process of our Micro-DL architecture. The effect of the scale coefficient on the clustering performances (e.g. Accuracy, Jac, FM and Rand) are shown in Fig. 5. From the results, we can obtain that the clustering performances increase as the scale coefficient is increased from 0.1 to 0.3. Then the performances begin to decline as α is increased from 0.4 to 0.9.

5 CONCLUSIONS

We have presented Micro-DL, a micro-supervised deep representation learning architecture based on two variant models (Micro-DGRBM and Micro-DRBM), which firstly introduced small-perturbation ideology on the representation learning model from the perspective of the representation probability distributions. The positive SPI stimulated the representation probability distributions of Micro-DGRBM and Micro-DRBM models to become more similar and dissimilar in the same and different clusters, respectively. Furthermore, the representation learning capability of Micro-DL has significantly enhanced under the continuous stimulation of SPI. The Micro-DL method improved the stability of representation learning from the perspective of representation probability distribution and significantly reduced the reliance on

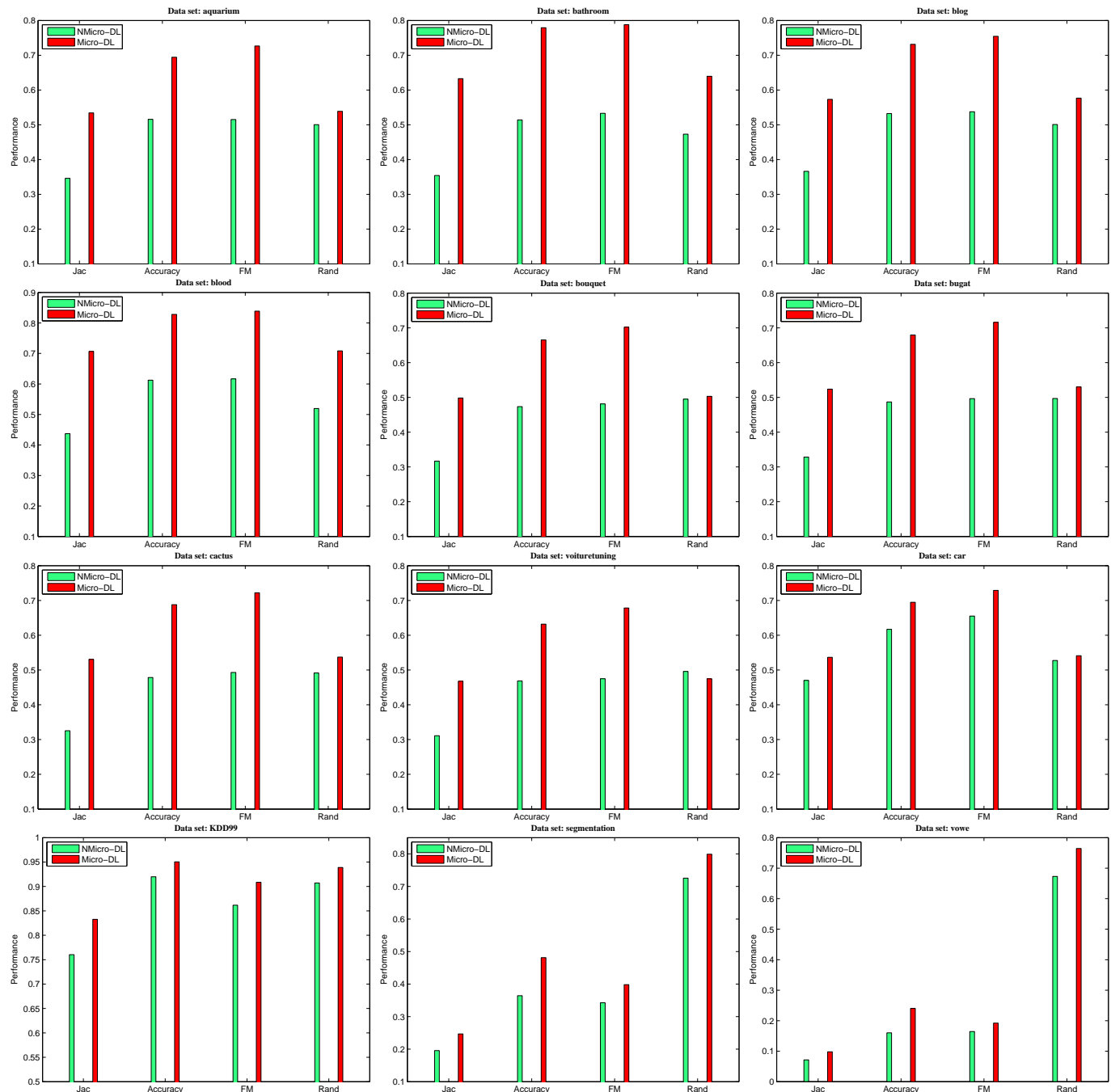


Fig. 4: The effectiveness of the SPI.

the labels. Experimental results demonstrated that the proposed deep Micro-DL architecture shows better performance in comparison to the baseline method, the most related shallow models and deep frameworks for clustering on twelve data sets.

In the future, there are several interesting works: 1) to introduce small-perturbation ideology on the other neural networks; 2) to study Micro-supervised representation method with single label in each cluster; 3) to explore the performance of Micro-DL on large-scale datasets.

6 ACKNOWLEDGEMENT

This work was supported by the National Science Foundation of China (Nos. 62176221, 71901158, 61876158, 61806170) and

Sichuan Science and Technology Program (2021YFS0178).

REFERENCES

- [1] Y. Bengio, A. Courville, and P. Vincent, "Representation learning: A review and new perspectives," *IEEE Transactions on Pattern Analysis and Machine Intelligence*, vol. 35, no. 8, pp. 1798–1828, 2013.
- [2] H. Yao, S. Zhang, R. Hong, Y. Zhang, C. Xu, and Q. Tian, "Deep representation learning with part loss for person re-identification," *IEEE Transactions on Image Processing*, vol. 28, no. 6, pp. 2860–2871, 2019.
- [3] M. Kutbi, K.-C. Peng, and Z. Wu, "Zero-shot deep domain adaptation with common representation learning," *IEEE Transactions on Pattern Analysis and Machine Intelligence*, pp. 1–1, 2021.

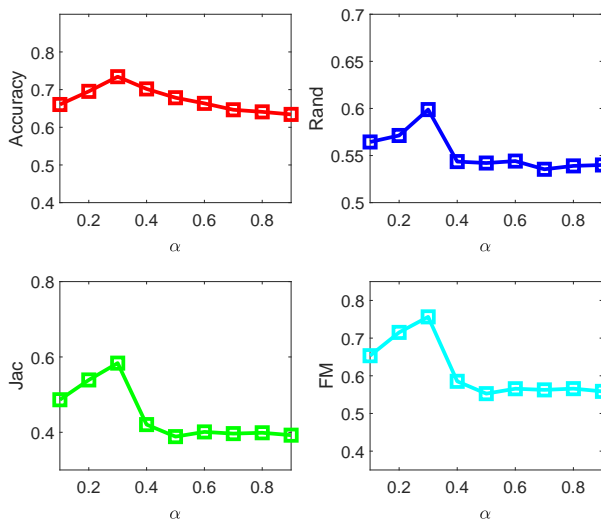


Fig. 5: Effect of the scale coefficient on the performance.

- [4] J. Wang, K. Sun, T. Cheng, B. Jiang, C. Deng, Y. Zhao, D. Liu, Y. Mu, M. Tan, X. Wang, W. Liu, and B. Xiao, "Deep high-resolution representation learning for visual recognition," *IEEE Transactions on Pattern Analysis and Machine Intelligence*, pp. 1–1, 2020.
- [5] J. J. Engelsma, K. Cao, and A. K. Jain, "Learning a fixed-length fingerprint representation," *IEEE Transactions on Pattern Analysis and Machine Intelligence*, vol. 43, no. 6, pp. 1981–1997, 2021.
- [6] H. Han, J. Li, A. K. Jain, S. Shan, and X. Chen, "Tattoo image search at scale: Joint detection and compact representation learning," *IEEE Transactions on Pattern Analysis and Machine Intelligence*, vol. 41, no. 10, pp. 2333–2348, 2019.
- [7] S. Ren, K. He, R. Girshick, and J. Sun, "Faster r-cnn: Towards real-time object detection with region proposal networks," *IEEE Transactions on Pattern Analysis and Machine Intelligence*, vol. 39, no. 6, pp. 1137–1149, 2017.
- [8] Y. Li, M. Yang, and Z. Zhang, "A survey of multi-view representation learning," *IEEE Transactions on Knowledge and Data Engineering*, vol. 31, no. 10, pp. 1863–1883, 2019.
- [9] Z. Yang, Q. Li, W. Liu, and J. Lv, "Shared multi-view data representation for multi-domain event detection," *IEEE Transactions on Pattern Analysis and Machine Intelligence*, vol. 42, no. 5, pp. 1243–1256, 2020.
- [10] S. Sun, W. Dong, and Q. Liu, "Multi-view representation learning with deep gaussian processes," *IEEE Transactions on Pattern Analysis and Machine Intelligence*, pp. 1–1, 2020.
- [11] M. Long, Y. Cao, Z. Cao, J. Wang, and M. I. Jordan, "Transferable representation learning with deep adaptation networks," *IEEE Transactions on Pattern Analysis and Machine Intelligence*, vol. 41, no. 12, pp. 3071–3085, 2019.
- [12] Y. Tamaazousti, H. Le Borgne, C. Hudelot, M.-E.-A. Seddik, and M. Tamaazousti, "Learning more universal representations for transfer-learning," *IEEE Transactions on Pattern Analysis and Machine Intelligence*, vol. 42, no. 9, pp. 2212–2224, 2020.
- [13] T. N. Kipf and M. Welling, "Variational graph auto-encoders," in *NIPS Workshop on Bayesian Deep Learning*, 2016.
- [14] R. A. Rossi, R. Zhou, and N. K. Ahmed, "Deep Inductive Graph Representation Learning," *IEEE Transactions on Knowledge and Data Engineering*, vol. 32, no. 3, pp. 438–452, MAR 1 2020.
- [15] Z. Zhang, L. Shao, Y. Xu, L. Liu, and J. Yang, "Marginal representation learning with graph structure self-adaptation," *IEEE Transactions on Neural Networks and Learning Systems*, vol. 29, no. 10, pp. 4645–4659, 2018.
- [16] B. Jiang, B. Wang, J. Tang, and B. Luo, "Gecns: Graph elastic convolutional networks for data representation," *IEEE Transactions on Pattern Analysis and Machine Intelligence*, pp. 1–1, 2021.
- [17] G. Giasemidis, N. Kaplis, I. Agrafiotis, and J. R. C. Nurse, "A semi-supervised approach to message stance classification," *IEEE Transactions on Knowledge and Data Engineering*, vol. 32, no. 1, pp. 1–11, Jan 2020.
- [18] C. Zhang, J. Cheng, and Q. Tian, "Unsupervised and semi-supervised image classification with weak semantic consistency," *IEEE Transactions on Multimedia*, vol. 21, no. 10, pp. 2482–2491, Oct 2019.
- [19] S. Liu, C. Ding, F. Jiang, Y. Wang, and B. Yin, "Auto-weighted multi-view learning for semi-supervised graph clustering," *Neurocomputing*, vol. 362, pp. 19 – 32, 2019.
- [20] Y. Ren, K. Hu, X. Dai, L. Pan, S. C. Hoi, and Z. Xu, "Semi-supervised deep embedded clustering," *Neurocomputing*, vol. 325, pp. 121 – 130, 2019.
- [21] J. Yang, S. Shebalov, and D. Klabjan, "Semi-supervised learning for discrete choice models," *IEEE Transactions on Intelligent Transportation Systems*, vol. 20, no. 11, pp. 4145–4159, Nov 2019.
- [22] S. Park, J. Lee, and K. Kim, "Semi-supervised distributed representations of documents for sentiment analysis," *Neural Networks*, vol. 119, pp. 139 – 150, 2019.
- [23] Z. Zeng, X. Wang, F. Yan, and Y. Chen, "Local adaptive learning for semi-supervised feature selection with group sparsity," *Knowledge-Based Systems*, vol. 181, p. 104787, 2019.
- [24] L. Li and Z. Zhang, "Semi-supervised domain adaptation by covariance matching," *IEEE Transactions on Pattern Analysis and Machine Intelligence*, vol. 41, no. 11, pp. 2724–2739, Nov 2019.
- [25] X. Chen, G. Yuan, F. Nie, and Z. Ming, "Semi-supervised feature selection via sparse rescaled linear square regression," *IEEE Transactions on Knowledge and Data Engineering*, vol. 32, no. 1, pp. 165–176, Jan 2020.
- [26] T. Ko and H. Kim, "Fault classification in high-dimensional complex processes using semi-supervised deep convolutional generative models," *IEEE Transactions on Industrial Informatics*, vol. 16, no. 4, pp. 2868–2877, April 2020.
- [27] X. Jia, X. Jing, X. Zhu, S. Chen, B. Du, Z. Cai, Z. He, and D. Yue, "Semi-supervised multi-view deep discriminant representation learning," *IEEE Transactions on Pattern Analysis and Machine Intelligence*, pp. 1–1, 2020.
- [28] Z. Chen, K. Wang, X. Wang, P. Peng, E. Izquierdo, and L. Lin, "Deep co-space: Sample mining across feature transformation for semi-supervised learning," *IEEE Transactions on Circuits and Systems for Video Technology*, vol. 28, no. 10, pp. 2667–2678, Oct 2018.
- [29] A. Sellami, M. Farah, I. R. Farah, and B. Solaiman, "Hyperspectral imagery classification based on semi-supervised 3-d deep neural network and adaptive band selection," *Expert Systems with Applications*, vol. 129, pp. 246 – 259, 2019.
- [30] B. Xue and N. Tong, "Diod: Fast and efficient weakly semi-supervised deep complex isar object detection," *IEEE Transactions on Cybernetics*, vol. 49, no. 11, pp. 3991–4003, Nov 2019.
- [31] Y. Meng, R. Shang, F. Shang, L. Jiao, S. Yang, and R. Stolkin, "Semi-supervised graph regularized deep nmf with bi-orthogonal constraints for data representation," *IEEE Transactions on Neural Networks and Learning Systems*, pp. 1–14, 2019.
- [32] P. Mercado, F. Tudisco, and M. Hein, "Generalized matrix means for semi-supervised learning with multilayer graphs," *NeurIPS*, pp. 14 848–14 857, 2019.
- [33] J. Chu, H. Wang, J. Liu, Z. Gong, and T. Li, "Unsupervised feature learning architecture with multi-clustering integration rbm," *IEEE Transactions on Knowledge and Data Engineering*, pp. 1–1, 2020.
- [34] J. Chu, H. Wang, H. Meng, P. Jin, and T. Li, "Restricted boltzmann machines with gaussian visible units guided by pairwise constraints," *IEEE Transactions on Cybernetics*, vol. 49, pp. 4321–4334, December 2019.
- [35] W. R. Sears, *SECTION C. SMALL PERTURBATION THEORY*. Princeton University Press, 2015, pp. 3–63. [Online]. Available: <https://doi.org/10.1515/9781400879021-002>
- [36] G. E. Hinton and R. R. Salakhutdinov, "Reducing the dimensionality of data with neural networks," *Science*, vol. 313, no. 5786, pp. 504–507, 2006.
- [37] P. Sankaran, S. Sunoj, and N. U. Nair, "Kullback-leibler divergence: A quantile approach," *Statistics and Probability Letters*, vol. 111, pp. 72 – 79, 2016.
- [38] G. E. Hinton, "Training products of experts by minimizing contrastive divergence," *Neural computation*, vol. 14, no. 8, pp. 1771–1800, 2002.
- [39] M. Jafar and K. Morteza, "Multiplicative distance: a method to alleviate distance instability for high-dimensional data," *Knowledge and Information Systems*, vol. 45, no. 3, pp. 783–805, 2015.
- [40] M. Ponti, J. Kittler, M. Riva, T. de Campos, and C. Zor, "A decision cognizant kullback-leibler divergence," *Pattern Recognition*, vol. 61, pp. 470 – 478, 2017.

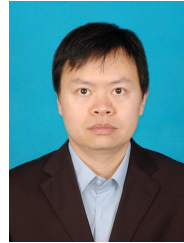
- [41] J. Collet, "An exact expression for the gap in the data processing inequality for f -divergences," *IEEE Transactions on Information Theory*, vol. 65, no. 7, pp. 4387–4391, July 2019.
- [42] P. Gurevich and H. Stuke, "Gradient conjugate priors and multi-layer neural networks," *Artificial Intelligence*, vol. 278, p. 103184, 2020.
- [43] K. K. Sharma and A. Seal, "Modeling uncertain data using monte carlo integration method for clustering," *Expert Systems with Applications*, vol. 137, pp. 100 – 116, 2019.
- [44] M. V. Giuffrida and S. A. Tsafaris, "Unsupervised rotation factorization in restricted boltzmann machines," *IEEE Transactions on Image Processing*, vol. 29, pp. 2166–2175, 2020.
- [45] A. Ahmadi and J. Tani, "A novel predictive-coding-inspired variational rnn model for online prediction and recognition," *Neural Computation*, vol. 31, no. 11, pp. 2025–2074, 2019.
- [46] M. A. Carreira-Perpinan and G. E. Hinton, "On contrastive divergence learning," in *Proceedings of the Tenth International Workshop on Artificial Intelligence and Statistics*. Citeseer, 2005, pp. 33–40.
- [47] Y. Freund and D. Haussler, *Unsupervised learning of distributions of binary vectors using two layer networks*. Computer Research Laboratory [University of California, Santa Cruz], 1994.
- [48] J. Zhang, G. Tian, Y. Mu, and W. Fan, "Supervised deep learning with auxiliary networks," in *Proceedings of the 20th ACM SIGKDD international conference on Knowledge discovery and data mining*. ACM, 2014, pp. 353–361.
- [49] H. Li, M. Wang, and X.-S. Hua, "Msra-mm 2.0: A large-scale web multimedia dataset," in *Data Mining Workshops, 2009. ICDMW'09. IEEE International Conference on*. IEEE, 2009, pp. 164–169.
- [50] S. S. Rangapuram and M. Hein, "Constrained 1-spectral clustering," *arXiv preprint arXiv:1505.06485*, 2015.
- [51] M. Wang, W. Fu, S. Hao, D. Tao, and X. Wu, "Scalable semi-supervised learning by efficient anchor graph regularization," *IEEE Transactions on Knowledge and Data Engineering*, vol. 28, no. 7, pp. 1864–1877, July 2016.
- [52] A. Y. Ng, M. I. Jordan, Y. Weiss *et al.*, "On spectral clustering: Analysis and an algorithm," *Advances in Neural Information Processing Systems*, vol. 2, pp. 849–856, 2002.
- [53] Y. Lin, J. Jiang, and S. Lee, "A similarity measure for text classification and clustering," *IEEE Transactions on Knowledge and Data Engineering*, vol. 26, no. 7, pp. 1575–1590, July 2014.
- [54] F. O. D. Franca, "A hash-based co-clustering algorithm for categorical data," *Expert Systems with Applications*, vol. 64, pp. 24–35, 2016.
- [55] R. Liu, H. Wang, and X. Yu, "Shared-nearest-neighbor-based clustering by fast search and find of density peaks," *Information Sciences*, vol. 450, pp. 200 – 226, 2018.
- [56] W. M. Rand, "Objective criteria for the evaluation of clustering methods," *Journal of the American Statistical Association*, vol. 66, no. 336, pp. 846–850, 1971.
- [57] S. García, A. Fernández, J. Luengo, and F. Herrera, "Advanced non-parametric tests for multiple comparisons in the design of experiments in computational intelligence and data mining: Experimental analysis of power," *Information Sciences*, vol. 180, no. 10, pp. 2044–2064, 2010.
- [58] C. Zhang and S. Ding, "A stochastic configuration network based on chaotic sparrow search algorithm," *Knowledge-Based Systems*, vol. 220, no. 10, p. 106924, 2021.



Jielei Chu received the B.S. and Ph.D. degrees in computer application and computer science and technology from Southwest Jiaotong University, Chengdu, China in 2008 and 2020. His research interests include deep learning, big data, semi-supervised learning and ensemble learning. He is a member of the IEEE.



Jing Liu received his Ph.D. degree in management from Southwest Jiaotong University. She is currently an Assistant Professor of Business School in Sichuan University. Her research interests are machine learning, financial technology and modelling and forecasting high-frequency data.



Hongjun Wang received his Ph.D. degree in Computer Science from Sichuan University of China in 2009. He is currently an Associate Professor of the Key Lab of Cloud Computing and Intelligent Techniques in Southwest Jiaotong University. His research interests include machine learning, data mining and ensemble learning. He has published over 50 research papers in journals and conferences and he is a member of ACM and CCF.



Meng Hua received his Ph.D. degree in Mathematics from Sichuan University of China in 2010. His research interests include belief revision, reasoning with uncertainty, machine learning, general topology.



Zhiguo Gong received the Ph.D. degree in Computer Science from the Institute of Mathematics, Chinese Academy of Science, Beijing, China. He is currently a Professor with the Faculty of Science and Technology, University of Macau, China. His current research interests include machine learning, data mining, database, and information retrieval.



Tianrui Li (SM'11) received the B.S., M.S., and Ph.D. degrees from Southwest Jiaotong University, Chengdu, China, in 1992, 1995, and 2002, respectively. He was a Post-Doctoral Researcher with Belgian Nuclear Research Centre, Mol, Belgium, from 2005 to 2006, and a Visiting Professor with Hasselt University, Hasselt, Belgium, in 2008; University of Technology, Sydney, Australia, in 2009; and University of Regina, Regina, Canada, in 2014. He is currently a Professor and the Director of the Key Laboratory of Cloud Computing and Intelligent Techniques, Southwest Jiaotong University. He has authored or co-authored over 300 research papers in refereed journals and conferences. His research interests include big data, machine learning, data mining, granular computing, and rough sets.